11

Structural Dynamic Behavior of Wind Turbines

Robert W. Thresher, Ph.D.
National Renewable Energy Laboratory
Golden, Colorado

Louis P. Mirandy, Ph.D.
The General Electric Company
King of Prussia, Pennsylvania

Thomas G. Carne, Ph.D. **Donald W. Lobitz, Ph.D.**
Sandia National Laboratories
Albuquerque, New Mexico

and

George H. James III, Ph.D.
NASA Johnson Space Center
Houston, Texas

Introduction

The structural dynamicist's areas of responsibility require interaction with most other members of the wind turbine project team. These responsibilities are to *predict structural loads and deflections* that will occur over the lifetime of the machine, *ensure favorable dynamic responses* through appropriate design and operational procedures, *evaluate potential design improvements* for their impact on dynamic loads and stability, and *correlate load and control test data* with design predictions. Load prediction has been a major concern in wind turbine designs to date, and it is perhaps the single most important task faced by the structural dynamics engineer. However, even if we were able to predict all loads perfectly, this in itself would not lead to an economic system. Reduction of dynamic loads, not merely a "design to loads" policy, is required to achieve a cost-effective design.

The two processes of load prediction and structural design are highly interactive: loads and deflections must be known before designers and stress analysts can perform structural sizing, which in turn influences the loads through changes in stiffness and mass. Structural design identifies "hot spots" (local areas of high stress) that would benefit most from dynamic load alleviation. Convergence of this cycle leads to a turbine structure that is neither under-designed (which may result in structural failure), nor over-designed (which will lead to excessive weight and cost).

This chapter introduces some of the physical principles and basic analytical tools needed for the structural dynamic analysis of a horizontal-axis or vertical-axis wind turbine (HAWT or VAWT). This is done through discussions of two subjects that are fundamental building blocks of our understanding of the structural-dynamic behavior of wind turbines:

- **Single-degree-of-freedom dynamic load model of a HAWT blade,** following the development of the *FLAP* computer code at the National Renewable Energy Laboratory [Thresher *et al.* 1986, Wright *et al.* 1988];
- **Theoretical and experimental analysis of the vibration modes of a VAWT system,** following methods developed at the Sandia National Laboratories [Carne *et al.* 1982].

These discussions are written for engineers familiar with structural mechanics, but no specific knowledge of wind turbine rotors is required. Other technical disciplines with which the wind turbine structural dynamicist should become familiar are *aerodynamics* (required to determine wind forces and *aeroelastic* effects), *rotor dynamics* (with its own special set of accelerations and responses), *statistics* (required in dealing with wind turbulence and fatigue life prediction), *mathematical modeling*, and *testing.*

Role of Structural Dynamics in the Overall System Design

The design cycle in a typical wind turbine project is usually divided into *concept definition* and *detail design* stages. During the concept definition period trade studies are conducted to determine the overall configuration. The structural dynamics engineer is concerned most with the relative load levels and the operational and technological risks associated with the various design alternatives. Initially, only the feasibility of each concept is judged, with little time spent on refinements. For example, aeroelastic stability might be addressed only for unconventional concepts where experience is lacking.

In the detail design stage the structural dynamicist must furnish the design loads and determine design and operational requirements that insure acceptable dynamic behavior. These requirements might include drive train damping and spring rates, balance tolerances, stiffness ranges for bearings, maximum operating wind speed, allowable yaw misalignment, yaw rate limits, etc., all based on the results of analysis using various mathematical models.

The key objectives that the design team seeks to achieve by relying on the guidance and skill of the structural dynamicist include the following:

- To select a configuration and design approach which alleviate dynamic loads
- To minimize the sensitivity of dynamic responses to inevitable differences between the "as-designed" and "as-built" physical properties of the structure
- To place natural frequencies favorably with respect to turbine operating speeds
- To insure aeroelastic stability, without which safe operation is impossible

Accomplishment of the first of these objectives must be based on the team's collective understanding of the dynamic behavior of various wind turbine configurations. It is guided

by past experience and frequently involves trade-offs with factors outside the realm of structural dynamics (*e.g.*, cost, manufacturing, and energy capture). The remaining key objectives are accomplished by straightforward (though sometimes complex) mathematical modelling of the selected configuration. Of course, the likelihood of a good detail design solution should be evident at the completion of the concept definition stage.

Wind Turbine Substructures and Subsystems

General background material on wind turbine nomenclature, configurations, and major substructures may be found in Chapters 2 and 3. It is its rotor which sets a wind turbine apart from other structural systems. Therefore, the thrust of this chapter is the understanding and analysis of wind turbines rotors. The structural dynamic behavior of the power train and support structures of a wind turbine can usually be analyzed by well-established methods, so these subsystems will not be discussed here.

Mathematical Models

While certain analyses can be accomplished with simple formulas, experience has shown that the analyst will need separate, specialized computer models to determine

- -- *System structural modes and natural frequencies* which incorporate rotational effects
- -- *System loads*, both steady-state and transient, incorporating all important degrees of freedom; includes deflections, vibrations, and power output quality
- -- *Aeroelastic stability*, including the effects of structure/control system interaction.

In theory, one comprehensive computer code could be used for all three of these tasks, but it might not be as efficient to develop or to run as separate specialized codes.

Modal Analysis Models

Modal analysis is the determination of the set of discrete patterns or *mode shapes*, each with at its own *modal frequency* and *modal damping*, which a vibrating structure describes. These patterns are also known as *natural modes*. Modal analysis of a wind turbine is generally based on well-developed *finite element* procedures (*e.g. NASTRAN*). Each substructure in the turbine system is modeled separately to determine its own mode shapes and frequencies. With special care, substructures can be coupled together to produce system modes. Modal models can be derived directly or spawned from more-detailed stress analysis models using standard *modal reduction* techniques. For rotors, centrifugal stiffening and gyroscopic effects can be incorporated directly into the finite element code, or they can be computed externally and applied later.

System Loads Model

The system loads code should be tailored to suit a specific wind turbine configuration, since a code that attempts to analyze all possible wind turbine types can become unwieldy. For example, the important dynamic loads usually result from motion in only a few dominant modes that are characteristic of a particular configuration, so the degrees of freedom used in the system loads model are generally a selected subset of the natural modes computed with the finite element models described above. While it is possible to use all of the finite-element degrees of freedom in the loads model, a modal approach is commonly used for analyzing system loads.

Direct numerical integration of the forced equations of motion in the time domain (*i.e.*, output is load *vs.* time) is the most straightforward and informative method of solution. This procedure, which is often referred to as *system simulation*, handles both steady-state and transient response. Since the governing equations of motion contain time-varying coefficients and are generally nonlinear, frequency domain techniques have limited value. Furthermore, seeking closed-form analytical solutions to these complex equations is usually unnecessary with the capabilities of today's digital computers. The engineer's time is best spent in understanding the results of a system simulation and then exploring methods for reducing dynamic loads.

Aeroelastic Stability Models

Aeroelastic stability analysis is often separate and distinct from the modal and loads analyses for two reasons: First, it is preferable to linearize the equations of motion and examine the resulting *eigenvalues* for stability, rather than to examine a myriad of time histories to determine if the response is stable. Of course, if the mechanism of instability is highly nonlinear, simulation in the time domain may be the only recourse. Most potential wind turbine instabilities can be adequately assessed using linearized models.

The second reason for a separate model is that the modes which are important for aeroelastic stability often differ from those needed for loads analysis. In a successful system, instabilities will occur outside the limits of planned operation. Hence, a blade torsional mode which incites instability at a high rotor speed may well be dormant during normal operation and, hence, be omitted in the loads analysis. It should be noted that aeroelastic stability analysis, like modal analysis, can be carried out with a finite-element model.

Dynamic Load Model of a HAWT Blade

A beam model of a wind turbine blade is generally suitable for structural-dynamic analysis. It will differ from the small-deflection theory beam models used in conventional analyses of non-rotating structures, however, because the axial loads on the blade significantly effect the lateral and torsional deflections. In this respect it is more like the beam-columns representations used in elastic stability analysis. General three-dimensional theory is quite complicated and has provided fodder for more than one doctoral thesis. It is still subject to controversy as to which terms are important and which are not. Rather than beginning with the general case, we will develop the equations for uncoupled *flapwise* (*i.e.* out-of-plane or flatwise) motions to acquaint the reader with the physics involved. In many cases, these will be suitable for the analysis of HAWT rotor loads.

Elastic blade flapping equations appear in many sources and are in a sense, classical. A relatively brief derivation is given here to highlight the approximations and assumptions that are implicit in the equations which are commonly used. We begin by assuming that the strains everywhere in the blade are small (less than 10%) and below the elastic limit. Other assumptions will be introduced at appropriate points in the derivation.[1] Equations of motion for wind turbine components are generally derived using a "strength of materials" rather than a "theory of elasticity" approach.

[1] Note here that the assumptions of small strain and elasticity do not mean that the deflections must be small. Everyone is aware that a steel ruler can be bent into an arc with deflections much greater than its cross-sectional dimensions, and yet it will spring back elastically to its original shape.

Coordinate System Definitions

Figure 11-1 shows the orientation of the HAWT blade under analysis with all the intermediate coordinates required to represent the blade motion. The *X-Y-Z* coordinates are the fixed reference system. The mean wind velocity at the hub elevation, V_{hub}, and its fluctuating components -- δV_X, δV_Y, δV_Z -- are given in this system. The rotor axis may be tilted at a fixed angle χ. It may also have a prescribed, time-dependent yawing motion given by the yaw angle $\phi(t)$. The yaw axis is coincident with the *Z*-coordinate axis. The center of the rotor hub, *H*, is located a distance *a* from the yaw axis. The blade may be rigid from the axis outward to a distance *h*, which may also be interpreted as the outer radius of the hub. The blade airfoil shape may begin at *h* or at a station further out along the blade *z* axis. The blade may be coned at a prescribed angle β_0, as shown in the figure.

The *x,y,z* coordinates are located in the surface of revolution that a rigid blade would trace in space, with the *y*-axis normal to this surface. The x_p-y_p-z_p system are the blade's principal bending coordinates, where the z_p-axis is coincident with the elastic axis of the undeformed blade. Bending takes place about the x_p-axis. It is further assumed that the blade principal axes of area inertia remain parallel along the z_p-axis. Any influence of blade twist on bending displacements is neglected. As a reference for computations, the angle θ_p is set equal to the orientation of the principal bending plane relative to the cone of rotation (*i.e.*, the *x*-*y*-*z* system) at a selected station of primary interest along the blade span. The third coordinate system illustrated in Figure 11-1 is the η-ζ-ξ system, which is on the principal axes of the deformed blade along each point along the elastic axis.

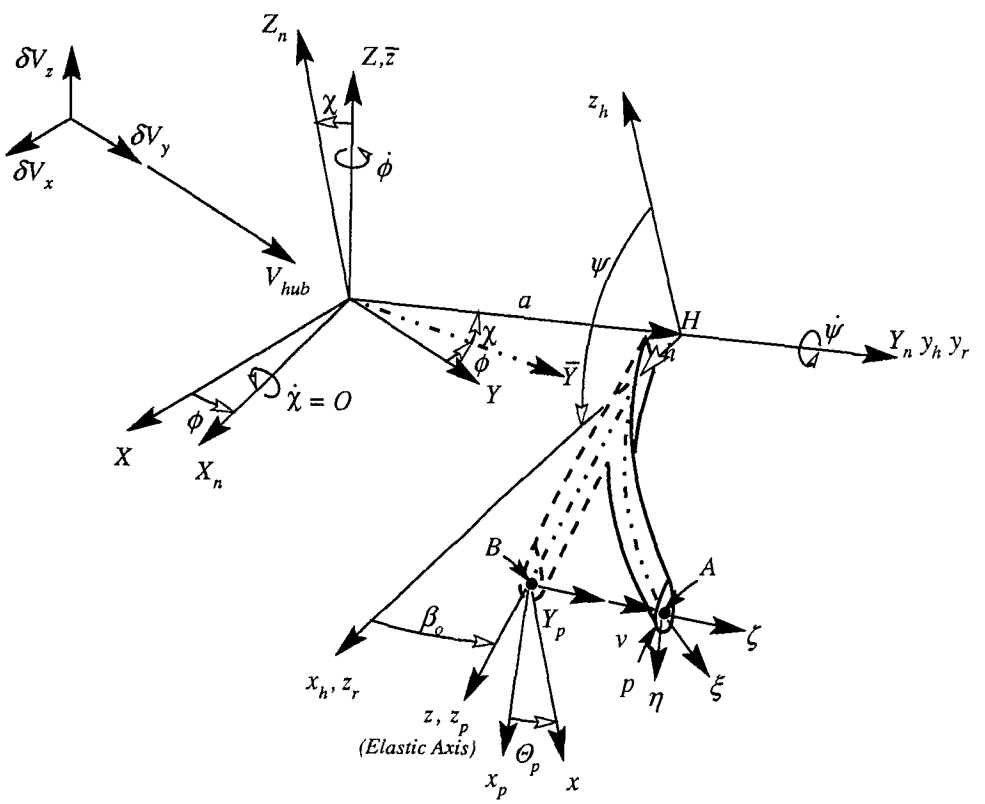

Figure 11-1. Fixed, rotating, and deformed-blade coordinate systems. Positive displacements and rotations are shown. [Wright et al. 1988]

The coordinate transformation that takes vector components from the fixed *X-Y-Z* system to the rotating x_p-y_p-z_p coordinates of the undeformed blade is as follows:

$$\begin{bmatrix} x_p \\ y_p \\ z_p \end{bmatrix} = \begin{bmatrix} a_{11} & a_{12} & a_{13} \\ a_{21} & a_{22} & a_{23} \\ a_{31} & a_{32} & a_{33} \end{bmatrix} = \begin{bmatrix} X \\ Y \\ Z \end{bmatrix} \tag{11-1}$$

where

$$\begin{aligned}
a_{11} &= c\theta_p c\psi + \beta_0 s\theta_p s\psi + \phi s\theta_p \\
a_{12} &= c\theta_p c\psi\phi - s\theta_p + \chi c\theta_p s\psi \\
a_{13} &= -\chi s\theta_p - c\theta_p s\psi + \beta_0 s\theta_p c\psi \\
a_{21} &= s\theta_p c\psi - \beta_0 c\theta_p s\psi - \phi c\theta_p \\
a_{22} &= s\theta_p c\psi\phi + c\theta_p + \chi s\theta_p s\psi \\
a_{23} &= \chi c\theta_p - s\theta_p s\psi - \beta_0 c\theta_p c\psi \\
a_{31} &= s\psi \\
a_{32} &= \phi s\psi + \beta_0 - \chi c\psi \\
a_{31} &= c\psi \\
c\theta_p &= \cos\theta_p \\
c\psi &= \cos\psi \\
s\theta_p &= \sin\theta_p \\
s\psi &= \sin\psi
\end{aligned}$$

This transformation has been linearized by assuming a small yaw angle ϕ, a small tilt angle χ, and a small coning angle β_0. The angle of the principal axis, θ_p, may be large. Of course, the blade azimuth angle, ψ, can vary from 0 to 2π radians. The inverse transformation taking the x_p-y_p-z_p components into the *X-Y-Z* system is given by the transpose of the 3x3 matrix in Equation (11-1). The blade position for $\psi = 0$ is straight up.

Assuming small deformations, the transformation for obtaining η-ζ-ξ components is

$$\begin{bmatrix} \eta \\ \zeta \\ \xi \end{bmatrix} = \begin{bmatrix} 1 & 0 & 0 \\ 0 & 1 & -v' \\ 0 & v' & 1 \end{bmatrix} \begin{bmatrix} x_p \\ y_p \\ z_p \end{bmatrix} \tag{11-2}$$

The necessary intermediate coordinate transformations for components in the x-y-z, x_r-y_r-z_r, and x_h-y_h-z_h coordinate systems shown in Figure 11-1 can be obtained as follows:

-- Set $\theta_p = 0$ for transforming to the x-y-z system;
-- Set $\theta_p = \beta_0 = 0$ for transforming to the x_r-y_r-z_r system;
-- Set $\theta_p = \beta_0 = \psi = 0$ for transforming to the x_h-y_h-z_h system.

Moment-Curvature Relationship

The HAWT blade is assumed to be a long, slender beam so that the normal strength-of-materials assumptions concerning the bending deformations are valid. Figure 11-2 shows an infinitesimal element of the deformed blade. It is assumed that the blade bends only about its weakest principal axis of inertia, which is about the x_p-axis in the figure. No other deformations are considered in this analysis. The strength-of-materials model for elastic bending assumes a one-dimensional form for Hooke's Law that neglects all stresses except the longitudinal (in this case *spanwise*) bending stress. It results in the following differential equation relating bending moment to curvature in our blade:

$$M_{x,p} = -EI_{x,p}\frac{d^2v}{dz_p^2} - EI_{x,p}v'' \tag{11-3}$$

where

$M_{x,p}$ = bending moment about the blade principal axis of inertia, x_p (N-m)
$[\,]' = d[\,]/dz_p$, *etc.*
E = modulus of elasticity (N/m^2)
$I_{x,p}$ = area moment of inertia of the airfoil section about the x_p-axis (m^4)
v = displacement in the y_p (flap) direction (m)

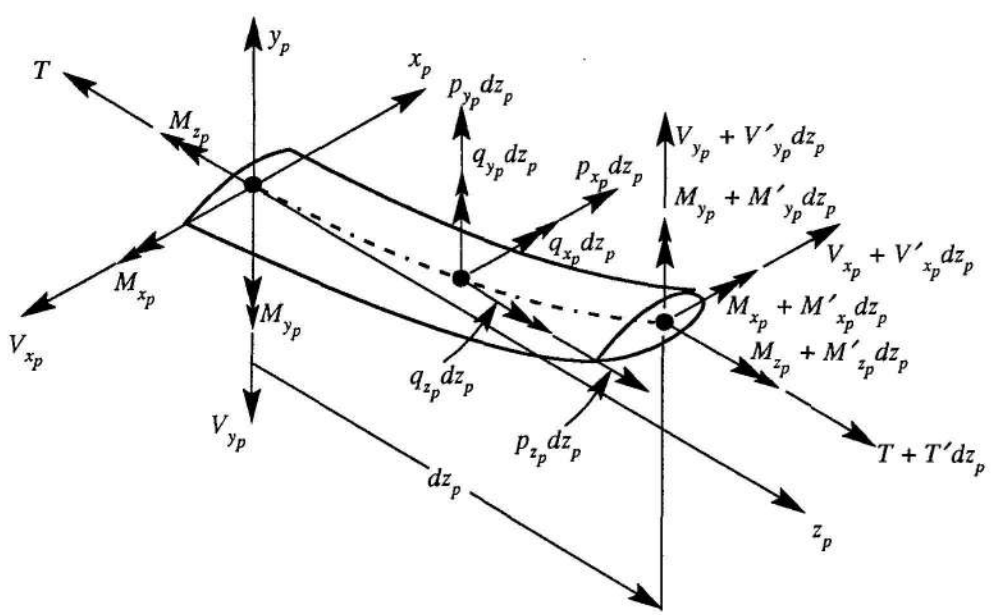

Figure 11-2. Deformed blade element showing forces and moments, all acting in a positive sense. [Wright *et al.* 1988]

Equilibrium Equations

The equations of equilibrium are derived by summing forces and moments in the three coordinate-axis directions and equating the sums to zero. Referring to Figure 11-2, summing of forces and moments gives the following six equations:

$$V'_{x,p} + p_{x,p} = 0 \tag{11-4a}$$

$$V'_{y,p} + p_{y,p} = 0 \tag{11-4b}$$

$$T' + p_{z,p} = 0 \tag{11-4c}$$

$$M'_{x,p} - V_{y,p} + Tv' + q_{x,p} = 0 \tag{11-5a}$$

$$M'_{y,p} + V_{x,p} + q_{y,p} = 0 \tag{11-5b}$$

$$M'_{z,p} - V_{x,p}\, v' + q_{z,p} = 0 \tag{11-5c}$$

where

$p_{x,p}, p_{y,p}, p_{z,p}$ = applied (external) force loading per unit length (N/m)
$q_{x,p}, q_{y,p}, q_{z,p}$ = applied (external) moment loading per unit length (N-m/m)
$M_{x,p}, M_{y,p}, M_{z,p}$ = internal bending moment loads (N-m)
$V_{x,p}, V_{y,p}, T$ = internal force loads (N)

The terms *load* and *loading* are often used interchangeably in the literature, so some clarification of their use in this chapter (and generally in this book) is in order. We shall use the term *loading* to describe an external action applied onto the structure. Thus, p and q are the sum of all aerodynamic pressures and inertial body forces and are here called *loadings*. The internal moment and force responses of the structure to these loadings -- M, V, and T -- are termed *loads*. It has become the general practice in the structural analysis of wind turbines that if the term "load" stands alone it refers to internal moment and force responses.

Differentiation twice of Equation (11-3) and once each of Equations (11-5a) and (11-5b) allows these three equations to be combined with each other and with Equations (11-4a) and (11-4b) to eliminate $M_{x,p}$, $V_{x,p}$, and $V_{y,p}$. In addition, Equations (11-5b) and (11-5c) can be combined to eliminate the shear force load $V_{x,p}$. These eliminations reduce the previous seven equations to the following four combined moment-curvature-equilibrium equations in the four unknowns v, $M_{x,p}$, $M_{y,p}$, and T:

$$\textit{Flapwise Bending}: \quad (-v''EI_{y,p})'' + (Tv')' + q'_{x,p} + p_{y,p} = 0 \tag{11-6a}$$

$$\textit{Edgewise Bending}: \quad M''_{y,p} + q'_{y,p} - p_{x,p} = 0 \tag{11-6b}$$

$$\textit{Pitchwise Torsion}: \quad M'_{z,p} + M'_{y,p}v' + q_{y,p}v' + q_{z,p} = 0 \tag{11-6c}$$

$$\textit{Spanwise Tension}: \quad T' + p_{z,p} = 0 \tag{11-6d}$$

Wind Speed Models

Wind Shear Gradient

The vertical gradient in steady wind speed with elevation above and below the elevation of the rotor axis is often modeled by a simple power law (see Chapter 8) as

$$U(z) = U_H(z/H)^m \tag{11-7}$$

where

$U(z)$ = free-stream wind speed at elevation z (m/s)
U_H = free-stream wind speed at hub elevation (m/s)
z = elevation above ground level (m)
H = elevation of the rotor hub (m)
m = empirical wind shear exponent (same as α in Eq. (8-11))

The wind speed gradient may be described in polar coordinates centered at the hub elevation by a binomial series, as follows:

$$U(z) = U_H\left(\frac{r\cos\psi + H}{H}\right)^m = U_H[1 + W_S(r,\psi)] \tag{11-8}$$

$$W_S(r,\psi) \simeq m\left(\frac{r}{H}\right)\cos\psi + \frac{m(m-1)}{2}\left(\frac{r}{H}\right)^2\cos^2\psi \tag{11-9}$$

where

r = radial distance from the rotor axis (m)
W_s = wind shear shape function

In this series expression, powers of *r/H* higher than 2 have been neglected.

Tower Shadow Deficit

The presence of the tower causes a deficit in the wind speed, with the downwind reduction often referred to as *tower shadow* and the much-smaller upwind reduction as a *bow wave* effect. Here we shall refer to both as tower shadow. Neglecting any effects of retardation by the rotor, we will assume that the deficit has a spatial distribution of the form

$$\delta V_T(z,\psi) = -W_T(\psi)U(z)$$

$$W_T(\psi) = \begin{cases} t_0 + t_p\cos[p(\psi - \pi)] \\ \quad for\ \pi - \psi_0 \le \psi \le \pi + \psi_0 \\ 0 \quad elsewhere \end{cases} \tag{11-10}$$

$$p = k\pi/\psi_0 \tag{11-11}$$

where

δV_T = wind speed deficit caused by the tower (m/s)
W_T = tower shadow shape function
t_0, t_p = empirical scale constants
ψ_0 = half-angle of tower shadow sector (rad)
k = number of waves in the tangential profile of the shadow

The parameters t_0, t_p, ψ_0, and k are selected to give the desired approximation for the tangential profile of wind speed in a pie-shaped region with a central angle of $2\psi_0$, centered on a blade azimuth angle of π. For example, the shadow of a shell tower is often modeled as a $\sin^2$ function using the following parameter values:

$t_0 = t_p$ = one-half the maximum ratio of deficit to free-stream wind speed
$k = 1$

A truss tower with three legs produces a shadow with three peaks, and this is modeled by selecting $k = 3$.

Spatial Turbulence Model

As discussed in Chapter 8 and illustrated in Figures 8-16 and 8-29, small-scale turbulence (*i.e.* having significant spatial variations in wind speed within the swept area of the rotor) will cause a moving rotor blade to experience a wind power spectrum with peaks at multiples of the rotor speed. In effect, the blade will be subject to harmonic forcing functions with frequencies at integer multiples of its rotational speed, and it will respond dynamically to them. Estimating the amplitudes of these turbulence forcing functions is beyond the scope of this chapter and is, in fact, the subject of current research on wind characteristics. Here we will make provision for wind turbulence excitations and emphasize that the harmonic content of these excitations plays an important role in determining the structural-dynamic response of wind turbine blades.

We shall assume that the distribution of turbulence-induced variations in wind speed across the rotor swept area changes slowly compared to the period of rotor rotation, so our model will be non-uniform in space but uniform in time. In the general case illustrated in Figure 11-1, the wind turbulence will have components in all three of the *X*-*Y*-*Z* directions, and each of these may vary with position in the rotor disk area. Thus

$$\delta U(r, \psi, t) = \begin{bmatrix} \delta u(r, \psi, 0) \\ \delta v(r, \psi, 0) \\ \delta w(r, \psi, 0) \end{bmatrix} \tag{11-12}$$

where

$\delta U(r,\psi,t)$ = turbulence in the free-stream horizontal wind (m/s)
$\delta u(r,\psi,0)$ = spatial turbulence in the X direction (m/s)
$\delta v(r,\psi,0)$ = spatial turbulence in the Y direction (m/s)
$\delta w(r,\psi,0)$ = spatial turbulence in the Z direction (m/s)

Induced (Retardation) Wind Speeds

In an unducted rotor, extraction of power reduces the speed of the wind at the rotor blades compared to the free-stream wind speed, as discussed in Chapter 5. This reduction is termed the *induced* wind speed and its magnitude is usually given as a fraction of the free-stream wind speed by a parameter called the *axial induction factor* (see Fig. 5-11). Calculation of axial induction factors is routinely performed using aerodynamic performance models, balancing the rate of change of the momentum in the wind stream with the rotor thrust. Because thrust is not normally uniform across the swept area of the rotor, advanced performance codes determine radial and circumferential distributions of the induction factors.

Some dynamic-load computer models also include the calculation of induced wind speeds. Whatever their source (*i.e.*, external or internal to the load model), provision must be made for induced wind speeds, because they can have a significant effect on airfoil angles of attack and on aerodynamic loading. In our wind model this is done as follows:

$$V_i(r, \psi) = a(r, \psi) U_H \tag{11-13}$$

where $a(r,\iota)$ = prescribed spatial distribution of axial induction factors

Combined Wind Effects

The net wind speed at point in the plane of rotation is the sum of free-stream, wind shear, tower shadow, turbulence, and induction components. These are usually combined in a linear fashion, neglecting minor interaction terms. To help avoid ill-conditioned simultaneous equations later, wind speeds are then normalized by the tip speed of the rotor. The net wind velocity vector is specified in the *X-Y-Z* coordinate system and is composed of steady and turbulence terms, as follows:

$$V_w(X - Y - Z) = R\Omega \begin{bmatrix} 0 \\ V_r + \delta V_r \\ 0 \end{bmatrix} + R\Omega \begin{bmatrix} \delta u \\ \delta v \\ \delta w \end{bmatrix} \tag{11-14a}$$

$$V_r = \frac{V_H[1 - a(r, \psi)]}{R\Omega} \tag{11-14b}$$

$$\delta V_r = \frac{V_H[W_S(r, \psi) - W_T(r, \psi)]}{R\Omega} \tag{11-14c}$$

$$\delta u = \delta u(r, \psi)/R\Omega \tag{11-14d}$$

$$\delta v = \delta v(r, \psi)/R\Omega \tag{11-14e}$$

$$\delta w = \delta w(r, \psi)/R\Omega \tag{11-14f}$$

where

$Vw(r, \iota)$ = net wind speed at the plane of rotation (m/s)
R = rotor tip radius (m)
Ω = rotor rotational speed (rad/s)

Kinematics of the Blade Motion

Velocity Analysis

We will now derive equations for the velocity of a point on the deformed blade in the η-ζ-ξ deformed blade system, starting in the *X-Y-Z* ground-based coordinate system and then transforming the results first into x_p-y_p-z_p principal blade coordinates and finally into the η-ζ-ξ coordinates. Referring to Figure 11-1, we can illustrate the required velocity vector analysis as follows: Designate the *X-Y-Z* coordinates as the α reference frame. Call the x_p-y_p-z_p principal blade coordinates, located at a point *B* on the elastic axis of the blade, as the β reference frame. The velocity of the same point on the deformed blade in the α system, here designated as *A*, may then be written symbolically as

$$\boldsymbol{V}_A(\alpha) = \boldsymbol{V}_B(\alpha) + \frac{d}{dt}\boldsymbol{r}_{A/B}(\beta) + \Omega x \boldsymbol{r}_{A/B} \qquad \text{Q1}$$

where subscript *A/B* indicates a vector from point *B* to point *A*. Performing the computations indicated by this equation and transforming the result the result using Equation (11-1) and then (11-2) gives

$$\boldsymbol{V}_A(\eta - \zeta - \xi) = R\Omega \begin{bmatrix} \boldsymbol{r}c\theta_p - \dot{\phi}[(\boldsymbol{d} + \beta_0\boldsymbol{r})c\theta_p + \boldsymbol{v}]c\psi - \dot{\phi}(\boldsymbol{r}s\theta_p)s\psi \\ \boldsymbol{r}s\theta_p + \dot{\boldsymbol{v}} - \dot{\phi}[(\boldsymbol{d} + \beta_0\boldsymbol{r})s\theta_p]c\psi + \dot{\phi}(\boldsymbol{r}c\theta_p)s\psi \\ (\boldsymbol{v}'\boldsymbol{r} - \boldsymbol{v})s\theta_p - \dot{\phi}[\boldsymbol{d} + (\boldsymbol{v} - \boldsymbol{v}'\boldsymbol{r})c\theta_p]s\psi \end{bmatrix} \qquad \text{(11-16a)}$$

$$\boldsymbol{r} = \frac{r}{R} \qquad \text{(11-16b)}$$

$$\dot{\phi} = \frac{\dot{\phi}}{\Omega} \qquad \text{(11-16c)}$$

$$\boldsymbol{d} = \frac{d}{R} \qquad \text{(11-16d)}$$

$$\boldsymbol{v} = \frac{v}{R} \qquad \text{(11-16e)}$$

where ϕ = yaw angle of the rotor axis (rad)
d = distance from the tower axis to the rotor hub (m)

and bold print designates a dimensionless variable. In addition, it has been assumed that the order of magnitude for the various terms are as follows:

$$\textit{Order 1 variables}: \quad \boldsymbol{r}$$
$$\textit{Order } \varepsilon_0^{1/2} \textit{ variables}: \quad \dot{\phi}$$
$$\textit{Order } \varepsilon_0 \textit{ variables}: \quad \boldsymbol{d}, \beta_0, \boldsymbol{v}, \dot{\boldsymbol{v}}, \boldsymbol{v}', H/R$$

Terms of order ε_0^2 and higher have been neglected in Equation (11-16a).

The relative velocity of the wind with respect to the moving rotor blade is computed by transforming the wind velocity components from Equation (11-14) into the deformed blade coordinates and then subtracting the blade velocity of Equation (1 l-16a). This gives

$$\frac{V_{rel}}{R\Omega} = \sqrt{\left(\frac{V_\eta}{R\Omega}\right)^2 + \left(\frac{V_\zeta}{R\Omega}\right)^2 + \left(\frac{V_\xi}{R\Omega}\right)^2} \tag{11-17a}$$

$$\frac{V_\eta}{R\Omega} = -\boldsymbol{r}c\theta_p - (\boldsymbol{V_r} + \delta \boldsymbol{V_r} + \delta \boldsymbol{V_y})s\theta_p + c\psi[(\delta \boldsymbol{V_x} + \phi \boldsymbol{V_r})c\theta_p + \dot{\phi}\{(\boldsymbol{d} + \beta_0 \boldsymbol{r})c\theta_p + \boldsymbol{v}\}] \tag{11-17b}$$

$$\frac{V_\eta}{R\Omega} = -\boldsymbol{r}s\theta_p - \dot{\boldsymbol{v}} + (\boldsymbol{V_r} + \delta \boldsymbol{V_r} + \delta \boldsymbol{V_y})c\theta_p + c\psi[(\delta \boldsymbol{V_x} + \phi \boldsymbol{V_r})s\theta_p + \dot{\phi}\{(\boldsymbol{d} + \beta_0 \boldsymbol{r})s\theta_p\}] + s\psi\{-(\delta \boldsymbol{V_z} - \chi \boldsymbol{V_r})s\theta_p - \dot{\phi}(\boldsymbol{r}c\theta_p)\} \tag{11-17c}$$

$$\frac{V_\zeta}{R\Omega} = -(\boldsymbol{v}'\boldsymbol{r} - \boldsymbol{v})s\theta_p + c\psi(\delta \boldsymbol{V_z} - \chi \boldsymbol{V_r}) + (\beta_0 + \boldsymbol{v}'c\theta_p)\boldsymbol{V_r} + s\psi[\delta \boldsymbol{V_x} + \phi \boldsymbol{V_r} + \dot{\phi}\{\boldsymbol{d} + (\boldsymbol{v} - \boldsymbol{v}'\boldsymbol{r})c\theta_p\}] \tag{11-17d}$$

where

V_{rel} = relative wind speed at airfoil section in η-ζ-ξ coordinates (m/s)
V_η = relative chordwise wind speed at airfoil section (m/s)
V_ζ = relative normal wind speed at airfoil section (m/s)
V_ξ = relative spanwise wind speed at airfoil section (m/s)

Terms of order ε_0^2 have been discarded in these equations. The following assumptions have been made regarding the order of the velocity components:

Order 1 *velocities*: $\boldsymbol{V_r}$
Order ε_0 *velocities*: $\delta \boldsymbol{V_r}, \delta \boldsymbol{V_x}, \delta \boldsymbol{V_y}, \delta \boldsymbol{V_z}$

Acceleration Analysis

Referring again to Figure 11-1, our acceleration analysis will recognize the fact that the mass of the blade is not all concentrated on the elastic axis but is distributed across the airfoil section. Acceleration equations will, therefore, be derived for an arbitrary point *P* at coordinates (η,ζ) within the cross-section. The point *A* in the velocity analysis is the same as *P*(0,0). Using the same α-β reference frame designations as for the velocity vector analysis, the acceleration of *P* is given by the usual five-term acceleration equation as

$$\boldsymbol{a_P}(\alpha) = \boldsymbol{a_B}(\alpha) + \frac{d\Omega}{dt} x \boldsymbol{r_{P/B}} + 2\Omega x \frac{d}{dt}\boldsymbol{r_{P/B}}(\beta) + \Omega x(\Omega x \boldsymbol{r_{P/B}}) + \frac{d^2}{dt}\boldsymbol{r_{P/B}} \qquad (11\text{-}18)$$

The indicated operations of Equation (11-18) must be carried out, and the results must then be transformed to the β coordinate system and linearized. This tedious activity gives the expressions for the acceleration components in the x_p-y_p-z_p coordinates. For the small-deformation theory of this analysis, there is no difference between the x_p-y_p-z_p and η-ζ-ξ coordinate systems with respect to structural equations. For convenience, therefore, we will use the same η-ζ-ξ notation for the accelerations as for the relative velocities. This gives

$$\boldsymbol{a_P} = \begin{bmatrix} a_{P,\eta} \\ a_{P,\zeta} \\ a_{P,\xi} \end{bmatrix} \qquad (11\text{-}19a)$$

$$a_{P,\eta} = -s\theta_p(r\Omega^2\beta_0 + 2\dot{\phi}\,\Omega rc\psi + \ddot{\phi} rs\psi + v\Omega^2 c\theta_p) - \zeta\Omega^2 c\,\theta_p s\theta_p - \eta\Omega^2 c\,\theta_p^2 \qquad (11\text{-}19b)$$

$$a_{P,\zeta} = -c\theta_p(r\Omega^2\beta_0 + 2\,\dot{\phi}\Omega rc\psi + \ddot{\phi} rs\psi) - v\Omega^2 c\theta_p^2 - \zeta\,\Omega^2 s\theta_p^2 - \eta\,\Omega^2 s\theta_p c\theta_p + \ddot{v} \qquad (11\text{-}19c)$$

$$a_{P,\xi} = -r\Omega^2 - 2\Omega\dot{v}s\theta_p \qquad (11\text{-}19d)$$

where

$a_{P,\eta}, a_{P,\zeta}, a_{P,\xi}$ = components of the acceleration vector at an arbitrary point P within the blade, in the normal, chordwise, and spanwise directions, respectively (m/s^2)

Aerodynamic Loading

Referring to Figure 6-1, the lift and drag forces on an airfoil section are given by

$$dL = \frac{1}{2}\rho\, C_L c\, V_{rel}^2 d\xi$$

$$dD = \frac{1}{2}\rho\, C_D c V_{rel}^2\, d\xi$$

where

dL = increment of lift force, normal to the relative wind (N)
dD = increment of drag force, parallel to the relative wind (N)
ρ = air density (kg/m^3)

C_L, C_D = lift and drag force coefficients, respectively; prescribed functions of α
α = angle of attack, from the relative wind to the chord line (rad)
c = chord length of the airfoil section (m)
$d\xi$ = increment of spanwise length (m)

We see from Figure 6-1 that the directions of the lift and drag forces are determined by the direction of the relative wind and not by the blade geometry. As a result, lift and drag directions will vary along the span of the blade and change with changing wind and operating conditions, which is not convenient for structural analysis.

The force components of interest for structural analysis are those related to the principal inertia axes of the entire blade. To locate these directions, we first define a *reference station* along the spanwise axis of the blade. The reference station is any location of special structural or aerodynamic interest. Referring to Figure 11-3, the angle between the cone of rotation and the chordline at this reference station is defined here as the *pitch angle*, θp.

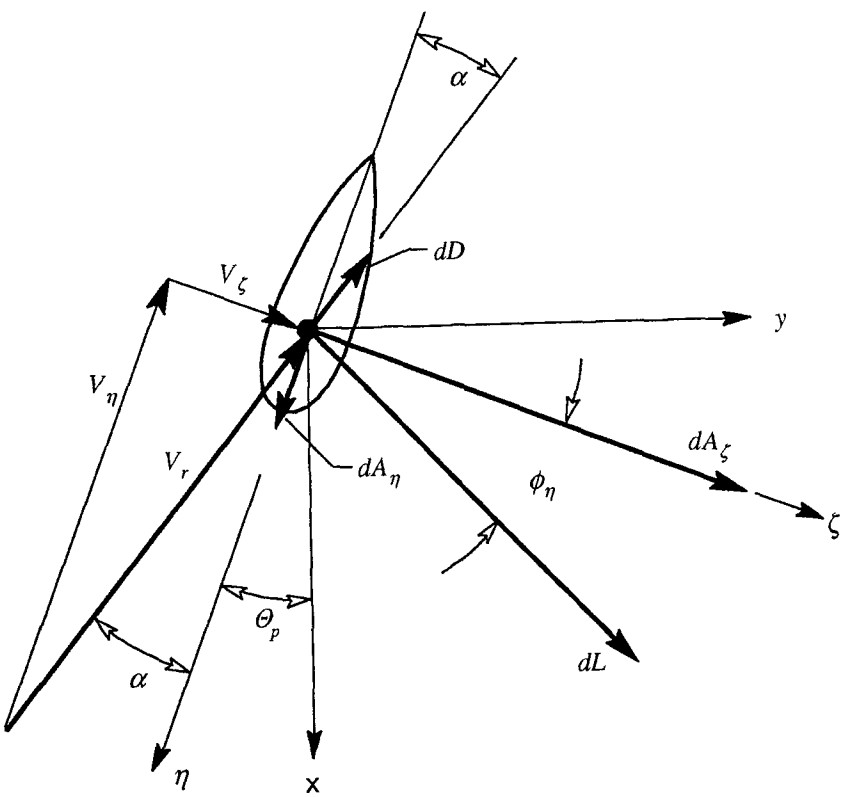

Figure 11-3. Velocity triangle at the blade reference station, and coordinate systems used for computing aerodynamic loading. The twist angle is zero. [Thresher *et al.* 1986]

The chord line at the reference station becomes the η-axis. Next, we define a *reference plane* as the surface generated by a η-axis line moving along the spanwise axis, remaining parallel to the chord line at the reference station. Finally, we define the *twist angle*, θ_t, as the angle between the local airfoil chord line and the reference plane. The force components of structural interest can now be expressed by

$$dA_\eta = \frac{1}{2}\rho c V_{rel}[C_L(\alpha)V_\zeta - C_D(\alpha)V_\eta]d\xi \tag{11-20a}$$

$$dA_\zeta = \frac{1}{2}\rho c V_{rel}[C_L(\alpha)V_\eta + C_D(\alpha)V_\zeta]d\xi \tag{11-20b}$$

$$\alpha = \theta_\eta - \theta_t \tag{11-20c}$$

$$\theta_\eta = \arctan(V_\zeta / V_\eta) \tag{11-20d}$$

where

dA_η, dA_ξ = increments of aerodynamic loading normal to and parallel to the blade reference plane (N/m)
θ_η = angle of the relative wind from the blade reference plane (rad)
θ_t = local twist angle relative to the blade reference plane; positive twist rotates the trailing edge downwind, as does positive pitch, θ_p (rad)

Most HAWT blades and their pitch control mechanism (if they have one) are relatively stiff in torsion about the spanwise axis, so aerodynamic pitching moments can be neglected. However, if a blade has pitch flexibility (*e.g.* one that is *self-twisting* for controlling power at high wind speeds) pitching moments must be included in the loading analysis, as follows:

$$q_{\xi,a} = \frac{1}{2}\rho c^2 V_{rel}^2 C_{M,a.c.} d\xi - e_{e.a.} c dA_\zeta \tag{11-21a}$$

$$e_{e.a.} = \frac{x_{a.c.} - x_{e.a.}}{c} \tag{11-21b}$$

where

dM_ζ = increment of aerodynamic pitch moment loading (N-m)
$C_{M,a.c.}$ = pitch moment coefficient about the aerodynamic center of the airfoil
e_{ea} = relative eccentricity of the elastic center of the airfoil; positive for elastic center between leading edge and aerodynamic center
x_{ac} = distance from leading edge to aerodynamic center; usually $c/4$ (m)
x_{ec} = distance from leading edge to elastic center (m)

Inertia Loading

The distributed inertia forces and moments acting along a unit length of the blade can be computed using Newton's laws as follows:

$$\boldsymbol{p_I} = \int_{\xi-12}^{\xi+1/2} -\boldsymbol{a_p} dm = \int_{Section} \int -\boldsymbol{a_P}\rho_b d\eta d\zeta \tag{11-23}$$ Q2

$$\boldsymbol{q_I} = \int_{\xi-1/2}^{\xi+1/2} -\boldsymbol{r_c} \times \boldsymbol{a_P} dm = \int_{Section} \int (\boldsymbol{r_c} \times \boldsymbol{a_P})\rho_b d\eta d\zeta \tag{11-24a}$$

$$\boldsymbol{r_c} = \begin{bmatrix} \eta \\ \zeta \\ 0 \end{bmatrix} \tag{11-24b}$$

where

dm = mass of an incremental length of blade (kg)
ρ_b = average mass density of the blade section (kg/m^3)

If the force of gravity is considered as deriving from an acceleration in the -Z direction, it can be treated in a similar manner.

Distributed Loading on the Blade

The combined loading on a HAWT blade caused by aerodynamic forces, shaft rotation, yaw motion, and gravity are

$$p_\eta = dA_\eta + m[(r\Omega^2\beta_0 + 2\Omega\dot{\phi}rc\psi + \ddot{\phi}rs\psi)s\theta_p + v\Omega^2 s\theta_p c\theta_p + e_\eta\Omega^2 c\theta_p^2 + mg(\chi s\theta_p + c\theta_p s\psi - \beta_0 s\theta_p c\psi) \tag{11-25a}$$

$$p_\zeta = dA_\zeta + m[-(r\Omega^2\beta_0 + 2\Omega\dot{\phi}rc\psi + \ddot{\phi}rs\psi)c\theta_p + v\Omega^2 s\theta_p^2 + e_\eta\Omega^2 s\theta_p c\theta_p - \ddot{v}] + mg(-\chi c\theta_p + s\theta_p s\psi + \beta_0 c\theta_p c\psi) \tag{11-25b}$$

$$p_\xi = m(r\Omega^2 + 2\dot{v}\Omega s\theta_p) - mgc\psi$$
$$q_\eta = v'\Omega^2 s\theta_p^2 I_{\eta\eta}^m \tag{11-25c}$$

$$q_\zeta + -mr\Omega^2 e_\eta - v'\Omega^2 c\theta_p s\theta_p I_{\eta\eta}^m + mge_\eta c\psi \tag{11-25d}$$

$$q_\xi = q_{\xi,a} + \Omega^2 s\theta_p c\theta_p (I_{\zeta\zeta}^m - I_{\eta\eta}^m) + mge_\eta s\psi\theta_p \tag{11-25e}$$

$$m = \int_{Section} \rho_b d\eta\, d\zeta \tag{11-25f}$$

$$e_\eta = \frac{1}{m}\int_{Section}\int \rho_b \eta\, d\eta\, d\zeta \tag{11-25g}$$

$$I_{\eta\eta}^m = \int_{Section}\int \rho_b \zeta^2 d\eta\, d\zeta \tag{11-25h}$$

$$I_{\eta\eta}^m = \int_{Section}\int \rho_b \eta^2 d\eta\, d\zeta \tag{11-25i}$$

where

m = blade mass per unit length (kg/m)
e_η = η-coordinate of the section center of mass (m)
$I_{\zeta\zeta}^{\ m}$ = minimum mass moment of inertia of section, per unit length (kg-m)
$I_{\eta\eta}^{\ m}$ = maximum mass moment of inertia of section, per unit length (kg-m)

Governing Equation of Motion

For this single-degree-of-freedom system, with flap displacement v as the only dynamic motion, the standard equation of motion for an incremental length of the blade has the form

$$[M]\,\ddot{v} + [J]\dot{v} + [K]\,v = [L] \tag{11-26}$$

where

$[M]$ = mass function (kg/m)
$[J]$ = damping function (N-s/m^2)
$[K]$ = stiffening function (N/m^2)
$[L]$ = loading function (N/m)

To develop this equation governing flap motion, it is necessary to begin with Equations (11-6) defining the equilibrium-moment curvature relationships for a blade element. Equation (11-6a) for flapwise bending will be converted into an equation of motion.

Spanwise Tension

The spanwise tension, T, in Equation (11-6a) can be obtained by directly integrating Equation (11-6d) to give

$$T(\xi) = \int_{\xi}^{R} m(r\Omega^2 + 2\dot{v}\Omega s\theta_p - gc\psi)d\xi \tag{11-27}$$

For the integration limit, we neglect any difference between the tip radius R and the length of the blade.

Modal Flap Displacement Model

In order to reduce the flap motion equation to an ordinary differential equation required for a computerized solution, a *modal model* is used, in which the flap displacement is assumed to be of the form

$$v(\xi, t) = \sum_k s_k(t)\gamma_k(\xi) \qquad k = 1, 2, \ldots \tag{11-28}$$

where

k = number of *mode shapes* in the displacement model
s_k = time-dependent displacement scaling factor for the kth mode (m)
γ_k = spanwise shape function for the kth mode

The spanwise shape functions, which must satisfy the blade kinematic and natural (force) boundary conditions, are usually prescribed as the mode shapes for free vibration of the

blade. The time-history of $s_k(t)$ is determined by numerical integration of the equation of motion during consecutive revolutions of the rotor, until each s_k and its first time derivative at $\psi = 2\pi$ are equal to the same parameters at $\psi = 0$, within a set tolerance. This is the so-called *trim solution.*

The flap mode shapes of importance to the structural-dynamic analysis of HAWT rotors can be divided into the following two classes: (1) *dependent* blade modes, in which the motions of a given blade are constrained or influenced by the motions of another blade in the rotor, and (2) *independent* blade modes, in which the motions of a given blade can be analyzed separately from the other blades. An example of a dependent mode is the rigid-body teetering motion of two-bladed HAWT rotor, in which the mode shapes of opposite blades must always be antisymmetric and without curvature at the hub. Dependent blade motions will not be discussed further here because of the additional complexity introduced by the constraints at the hub. The reader is referred to Wright *et al.* [1988] and [Wright and Butterfield 1991] for the equations required to perform a dynamic analysis of a teetered HAWT rotor and sample comparisons with test data.

The two classic examples of independent blade modes are the *cantilevered* shape, in which both v and v' are zero at the hub, but v'' may be non-zero; and the *flapping hinge* shape, in which both v and v'' are zero at the hub, but v' may be non-zero [Spera 1975]. In the remainder of this analysis, we will limit ourselves to one independent flapwise mode, for simplicity (*i.e.*, $k = 1$). Fortunately, experience has shown that one cantilever flapwise mode is usually sufficient for the calculation of blade loads in a rigid-hub rotor. Moreover, blade loads are much more sensitive to the scale of the wind input models (for wind shear, turbulence, and tower-shadow) than they are to higher blade modes. The exception to this general observation is the case in which the natural frequency of the next-higher mode is equal to an integer multiple of the rotor speed, and a resonance condition may be present.

Equation of Motion for One Independent Blade Mode

Substitution of the assumed form of the blade displacement from Equation (11-28) into Equation (11-6a) with k set equal to 1 gives

$$[-(s\gamma)''EI_\xi]'' + (Ts\gamma')' + q'_\xi + p_\zeta = 0 \tag{11-29}$$

Now, using a *Galerkin* approach [*e.g.* Dym and Shames 1973] gives us

$$\int_0^R \left\{[-(s\gamma)''EI_\xi]'' + (Ts\gamma')' + q'_\xi + p_\zeta\right\}\gamma d\xi = 0 \tag{11-30}$$

Integrating this equation by parts and using the boundary conditions required of $\gamma(\xi)$ lead to an ordinary differential equation in $s(t)$, which can then be integrated numerically in the time domain.

The numerical integration approach is best explained by rearranging Equation (11-29) so that the acceleration term remains on the left-hand side but all other terms are moved to the right-hand side. If we perform our time-domain integration in time steps of duration dt, we can now calculate the acceleration at time t in terms of the right-hand side of the equation evaluated with calculations made previously at time $t - dt$. We continue this forward-integration process in time until convergence to a trim solution is obtained. As discussed previously, trim is achieved when the flap displacement and velocity at $\psi = 2\pi$ are equal to the same parameters at $\psi = 0$, within a specified tolerance.

Carrying out the integration of Equation (11-30) by parts gives the following expressions for the flap accelerations of an independent blade:

$$\ddot{s}M = -sK_B - s\left(\Omega^2 K_\Omega + 2\Omega s\theta_p \dot{s}K_C - c\psi g K_g\right)$$
(***Bending***) (***Tension Stiffening***)

$$-c\theta_p\left(\Omega^2 + 2\Omega\dot{\phi}c\psi + \ddot{\phi}s\psi\right)M_R$$
(***Rigid−Body Motion***)

$$+s\Omega^2 s\theta_p^2 K_q$$
(***Inertia Moment Stiffening***)

$$+\Omega^2 s\theta_p c\theta_p M_B \qquad + F_a \tag{11-31}$$
(***C.G. Imbalance***) (***Aero Forace***)

$$+ s\Omega^2 s\theta_p^2 M$$
(***Inertia Force Stiffening***)

$$+ g(-\chi c\theta_p + s\theta_p s\psi + \beta_0 c\theta_p c\psi)M_g$$
(***Gravity***)

The various coefficients in this acceleration equation are given by the integrals in Equations (11-32) which are evaluated numerically. A *trim* solution of the equation of motion is then found by forward integration in time (or, equivalently, in azimuth ψ) until the following *convergence criteria* are met:

$$s[2(n+1)\pi/\Omega] = s[2n\pi/\Omega] \pm \varepsilon_1$$
$$\dot{s}[2(n+1)\pi/\Omega] = \dot{s}[2n\pi/\Omega] \pm \varepsilon_2$$

where

n = number of rotor rotations
$\varepsilon_1, \varepsilon_2$ = convergence tolerances (m, m/s)

$$
\begin{aligned}
M &= \int_0^R m\gamma^2 d\xi \\
M_R &= \int_0^R mr\gamma d\xi \\
M_B &= \int_0^R e_\eta m\gamma d\xi \\
M_g &= \int_0^R m\gamma d\xi \\
K_B &= \int_0^R EI_\zeta(\gamma'')^2 d\xi \\
K_\Omega &= \int_0^R T_\Omega(\xi)(\gamma')^2 d\xi \\
K_q &= I_{\eta\eta}(R)\gamma'(R)\gamma(L) - \int_0^R I_{\eta\eta}(\gamma')^2 D\Xi \\
K_c &= \int_0^r T_c(\xi)(\gamma')^2 d\xi \\
F_a &= \int_0^R dA_\zeta \gamma d\xi \\
T_\Omega(\xi) &= \int_\xi^R mrd\xi \\
T_c(\xi) &= \int_\xi^{RT} m\gamma d\xi \\
T_g(\xi) &= \int_\xi^R md\xi)
\end{aligned}
\tag{11-32}
$$

After a trim solution has been found or after each revolution of a yaw-motion solution, the flap displacement, slope, and velocity can be computed from the following equations:

$$v = s(t)\gamma(\xi) \tag{11-33a}$$

$$v' = s(t)\gamma'(\xi) \tag{11-33b}$$

$$\dot{v} = \dot{s}(t)\gamma(\xi) \tag{11-33c}$$

Rotor Blade Loads

Blade loads distributed along the ξ-axis are calculated by *the force-integration* method, as follows: From Equations (11-27) and (11-32c), the spanwise tension force load is

$$T(\xi) = \Omega^2 T_\Omega(\xi) + 2\Omega s\theta_p \dot{s} T_c(\xi) - gc\psi T_g(\xi) \tag{11-33}$$

Q3

Integrating Equation (11-4b) gives the blade flapwise shear force load as

$$\begin{aligned} V_\zeta(\xi) = &\int_\xi^R dA_\zeta d\xi - (\Omega^2\beta_0 + 2\Omega\dot{\phi}c\psi + \ddot{\phi}s\psi)c\theta_p T_\Omega(\xi) \\ &+ (\Omega^2 s\theta_p^2 s - \ddot{s})T_c(\xi) + \Omega^2 s\theta_p c\theta_p M_e(\xi) \\ &+ g(-\chi c\theta_p + s\theta_p s\psi + \beta_0 c\theta_p c\psi)T_g(\xi) \end{aligned} \tag{11-34}$$

Integrating Equation (11-4a) gives the blade chordwise shear force load as

$$\begin{aligned} V_\eta(\xi) = &\int_\xi^R dA_\eta d\xi + (\Omega^2\beta_0 + 2\Omega\dot{\phi}c\psi + \ddot{\phi}s\psi)s\theta_p T_\Omega(\xi) \\ &+ \Omega^2 s\theta_p c\theta_p s T_c(\xi) + \Omega^2 c\theta_p^2 M_e(\xi) \\ &+ g(\chi s\theta_p + c\theta_p s\psi - \beta_0 s\theta_p c\psi)T_g(\xi) \end{aligned} \tag{11-35}$$

Integrating Equation (11-5c) gives the blade pitch moment load as

$$\begin{aligned} M_\xi(\xi) = &-\int_\xi^R V_\eta(\xi)v'(\xi)d\xi + \int_\xi^R q_{\xi,a}(\xi)d\xi \\ &-\Omega^2 s\theta_p c\theta_p \Delta I(\xi) + gs\psi s\theta_p M_e(\xi) \end{aligned} \tag{11-36}$$

Integrating Equation (11-5b) gives the blade edgewise moment load as

$$\begin{aligned} M_\zeta(\xi) = &\int_\xi^R V_\eta(\xi)d\xi - \Omega^2 \int_\xi^R e_\eta m(\xi)rd\xi \\ &-\Omega^2 c\theta_p s\theta_p s \int_\xi^R I_{\eta\eta}(\xi)d\xi + gc\psi M_e(\xi) \end{aligned} \tag{11-37}$$

Finally, integrating Equation (11-5a) gives the blade flatwise moment load as

$$M_\eta(\xi) = -\int_\xi^R V_\zeta(\xi)d\xi + \int_\xi^R T(\xi)v'(\xi)d\xi + \Omega^2 s\theta_p^2 s\int_\xi^R I_{\eta\eta}(\xi)\gamma'(\xi)d\xi \tag{11-38}$$

In the above equations,

$$M_e(\xi) = \int_\xi^R e_\eta(\xi)m(\xi)d\xi \tag{11-39a}$$

$$\Delta I(\xi) = \int_\xi^R [I_{\zeta\zeta}(\xi) - I_{\eta\eta}(\xi)]d\xi \tag{11-39b}$$

Typical Computer Model for Blade Load Calculations

The calculation of wind turbine blade loads for even the simplest of cases, such as the one described here (*i.e.*, one degree of freedom and one blade mode), requires a computer model. A variety of special-purpose models for HAWT loads have been developed in the past, dating back to the 1970s when only mainframe computers had sufficient capability for the task [Spera 1977]. Today, HAWT load computer models for personal computers are available, such as the FLAP Code [Wright *et al.* 1988]. The following discussion is based on experience with the FLAP Code, which is a current analysis tool in the public domain.

Requirements

A computerized solution of the equation of motion and computation of displacements and loads requires a sophisticated, interactive model that is flexible, well-documented, and easily modified. The model must be capable of performing a variety of tasks, including

- -- input of data and output of results;
- -- matrix inversion;
- -- time-domain analysis of differential equations;
- -- computation of spatially-dependent blade properties and aerodynamic parameters.

The computational requirements of the equation of motion and other quantities associated with it determine which portions of the model can forego efficiency in favor of flexibility and readability, and which portions need to be as efficient as possible. This can be accommodated in a computer model composed of two modules, as illustrated by the flow chart in Figure 11-4.

Module 1 is a data pre-processor, in which a file of raw blade and turbine property is processed to produce a data file that can be used to solve the equation of motion. Flexibility and readability are more important than efficiency in this module. Module 1 also computes all the coefficient matrices since they are independent of most of the non-structural variables, such as wind speed and tower shadow. Module 2 performs the actual model run including solution of the equation of motion, computation of the loads and output of the results. Here, efficiency is a primary requirement.

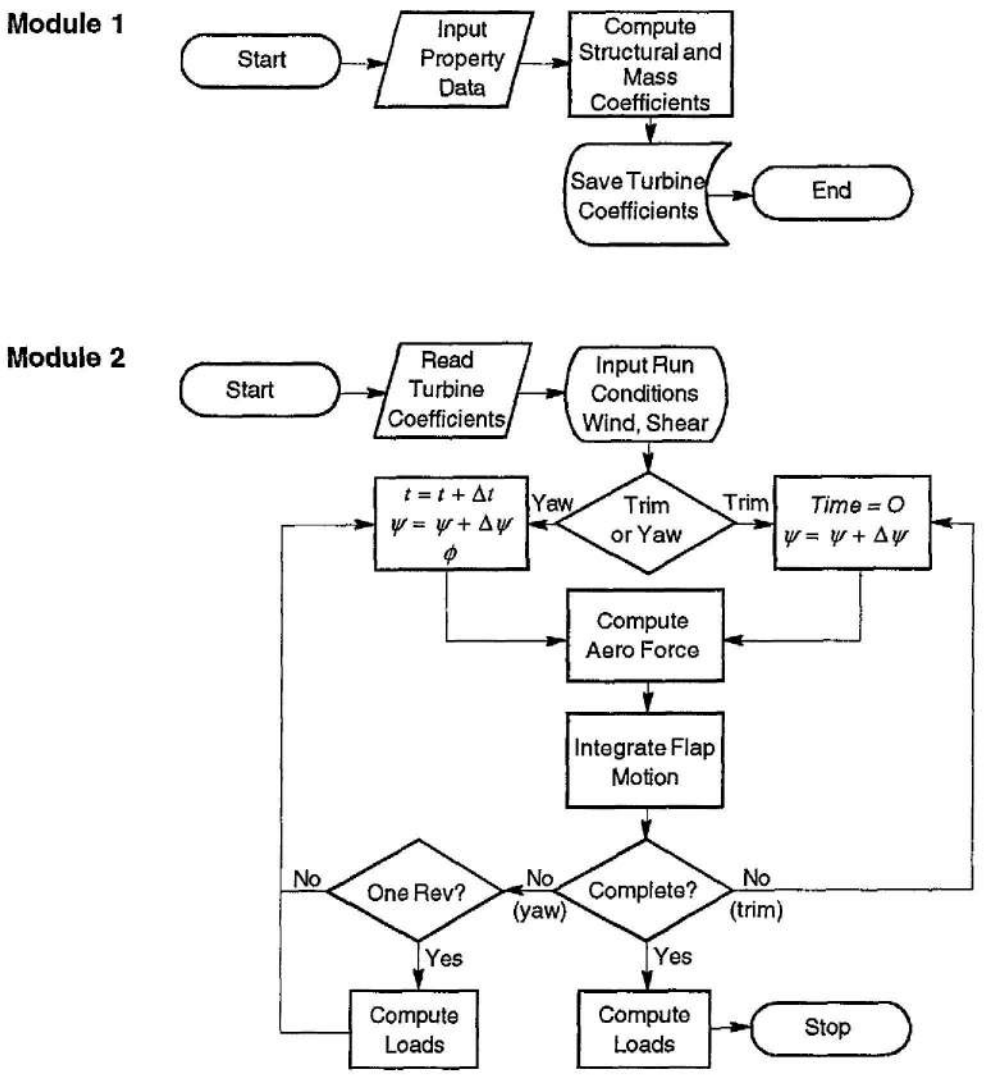

Figure 11-4. Typical flow chart for a computer model used to calculate HAWT blade loads. [Thresher *et al.* 1986]

Computational Procedure

The procedure followed in the FLAP Code for solving Equation (11-31), the fundamental equation of motion for a HAWT blade, can serve as an illustration of an approach that has been used successfully by the creators of such computer models. The general approach is as follows:

1. All coefficient matrices are multiplied by the inverse of the mass matrix. Thus the mass matrix associated with blade tip accelerations multiplied by its inverse gives the identity matrix. This results in a set of equations with the blade tip accelerations on one side of the equality and the computed generalized forces on the other. Multiplication by the inverse mass matrix is only done once, at the beginning of Module 2.

2. In this way, the accelerations associated with each flap coordinate function can be evaluated numerically be substituting the current values for the flap velocities and displacements into the force side of the equation.

3. The blade tip displacements are computed by solving the second-order differential equation relating acceleration, velocity, and displacement. The solution is performed *via* the modified Euler predictor-corrector method, which uses the current blade tip accelerations and the previous values of the displacements and velocities.

4. The blade loads are computed only at the completion of a trim solution.

5. The solution during time-dependent prescribed yawing motions is run at the completion of the trim solution. Loads are computed at the completion of each revolution during the yawing solution. Yawing motion is prescribed according to the simple equation

$$\phi(t) = \phi_0 + \phi_a \sin(\omega_\phi t) \tag{11-40}$$

6. A set of nine blade motion and blade load parameters is computed for each specified spanwise location on the blade axis (typically 11 stations) at each azimuthal position of the blade during a revolution (typically 36 azimuths). These parameters are the

   -- flap displacement, v;
   -- flapwise slope, v';
   -- flap velocity, dv/dt;
   -- edgewise shear load, S_η;
   -- flapwise shear load, S_ζ;
   -- spanwise tension load, T;
   -- flapwise moment load, M_η;
   -- edgewise moment load, M_ζ;
   -- pitching moment load, M_ξ.

Sample Blade Load Analysis

The turbine modeled in this example is the *Grumman* prototype HAWT (see Table 3-1), which has a three-bladed, rigid-hub rotor 10.1-m in diameter that runs downwind of a shell tower [Adler *et al.* 1980]. The lift and drag models are simplifications of the airfoil data presented by Sweeney and Nixon [1978]. Other input data are as follows:

U_H = 9.1 m/s	m = 0.143
t_0 = 0.25	t_p = 0
Ψ_0 = 15 deg	ϕ_0 = 10 deg
Ω = 7.54 rad/s	c = 0.46 m
β_0 = 3.5 deg	θ_t = 0 deg

The natural frequency of the blade's first (*i.e.* lowest frequency) flapwise bending mode is approximately 3.95 Hz, or about 3.3 times the rotor rotational frequency.

Flap bending moments in the operating turbine were measured at a spanwise station 1.8 m from the rotor axis (20% of span) and averaged over 20 revolutions. The test data were azimuth-averaged in this manner to remove random wind effects that are not modeled in this analysis. After averaging, the mean value of the measured flap bending moment was

subtracted, producing the variable flap moment history labeled "Test Data" in Figure 11-5. The calculated flap moment load at 20% of span, again with the average removed, is also plotted in Figure 11-5, permitting a comparison of the blade's flapping response to gravity, tower shadow, and average wind shear.

The test and calculated wave forms are very similar in Figure 11-5, indicating a validated computer model for this turbine. However, another HAWT would require a similar test/calculation comparison for validation of its structural, aerodynamic, and wind input data. These data are an integral part of the blade load analysis model, and as critical to validation as the basic equations of motion.

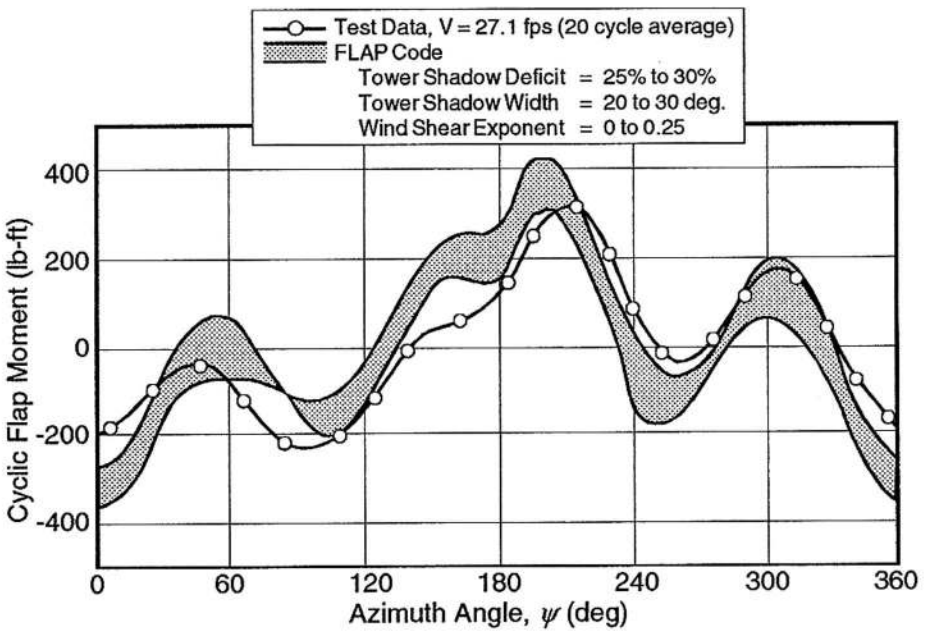

Figure 11-5. Sample comparison between calculated and measured flapwise moment loads. The test turbine is the 10.1-m diameter *Grumman* prototype HAWT. [Thresher *et al.* 1986]

Current and Future Developments in Structural-Dynamic Modeling

The demands placed on structural dynamics models are becoming more severe as turbine designs evolve. Models are being asked to account for more-complex phenomena, including

- non-steady air flow;
- blade-to-blade interactions;
- yaw and pitch motions of the nacelle and tower;
- blade pitch control;
- teetering motion;
- variable-speed;
- startup transient;
- shutdown and braking transients.

The desire to account for all such effects within one or two comprehensive models is driving engineers to develop computer codes of ever-increasing complexity.

Improved structural dynamic models of wind turbines appear to be developing along two different paths. The first approach involves *special purpose* codes, each written to analyze the structural dynamic behavior of a specific configuration of wind turbine. Such codes generally have 12 to 15 *degrees of freedom* (DOF) tailored to the significant motions of the "target" structural system. The second approach seeks to adapt *general purpose* structural analysis codes to simulate wind turbine dynamics. These general purpose codes are powerful enough to handle almost any turbine configuration, but they are complex and expensive. Moreover, the structural dynamicist must have a significant level of expertise in their use, and each new configuration requires considerable time for modeling and verification efforts.

Typical Special-Purpose Model

The structural analysis program *PHATAS-II*, developed at the *Netherlands Energy Research Foundation* (ECN), is an example of a current special-purpose code [Lindenburg and Snel 1993]. The PHATAS computer model can be used to calculate dynamic displacements and loads for the main structural subsystems of a HAWT. Wind inputs to this model include

- steady wind, including vertical and horizontal gradients;
- wind direction as a function of elevation;
- rotationally-sampled wind turbulence;
- turbulent wind in time-series form.

A number of structural degrees of freedom are available within the code, such as

- flapwise and chordwise elastic blade deformations;
- blade pitch motion;
- blade flapping and teetering hinges;
- torsional deflection of the power train;
- variable rotor speed;
- pitch and yaw motions of the nacelle;
- bending and torsional deflections of the tower.

Typical General-Purpose Model

The *ADAMS* code, developed at *Mechanical Dynamics, Inc.*, is an example of a general-purpose, multi-body structural analysis program that has been adapted for wind turbine applications [Malcolm and Wright 1994]. This code has virtually unlimited degrees of freedom and places no limits on the type or magnitude of displacements. While the ADAMS code can be run on a high-end personal computer (PC), it is exceptionally slow when modeling systems with many degrees of freedom or when performing simulations involving wind turbulence inputs. For example, it can take several days of PC run time to simulate 10 minutes of real time operation of a HAWT subjected to turbulent winds.

The strengths of this type of computer model are that almost any structural system (wind turbine or otherwise) can be modeled with it once the required skills have been learned by the user, and a mixture of complex external loadings and operating conditions can be applied. As PC performance increases, this type of general-purpose computer model is expected to used more and more for the structural analysis of modern wind turbines.

Natural Vibration Modes in a Wind Turbine

Dynamic effects can be substantial in a wind turbine system because of the periodic nature of its aerodynamic loading. As a result, the design process must depend on accurate predictive tools and/or measurement techniques for determining the dynamic response characteristics of the rotating structure. An elastic structure responds to periodic *forcing functions* by vibrating in one or more discrete geometric patterns called *mode shapes*, each of which has a companion rate of vibration called a *modal frequency*. Mode shapes and frequencies are determined primarily by the distributions of mass and stiffness throughout the structure and by its *boundary conditions*. Rotation can alter the natural frequencies of certain mode shapes, when centrifugal and Coriolis forces change stiffnesses. Because mode shapes and frequencies are relatively independent of applied loadings, they are often referred to as *natural* or *free-vibration modes*. Both analytical and experimental procedures for determining mode shapes and frequencies are referred to as *modal analysis*.

Figure 11-6 shows the results of a typical modal analysis of a HAWT [Sullivan 1981], displayed in a frequency plot called a *Campbell diagram*. Natural frequencies are plotted *vs.* rotational speed, with one generally-horizontal line per mode. Rays from the origin are plots of integer multiples of the rotational frequency. In a rotating structure, excitation loadings normally occur at these integer-multiple frequencies, often abbreviated 1*P*, 2*P*, *etc.*

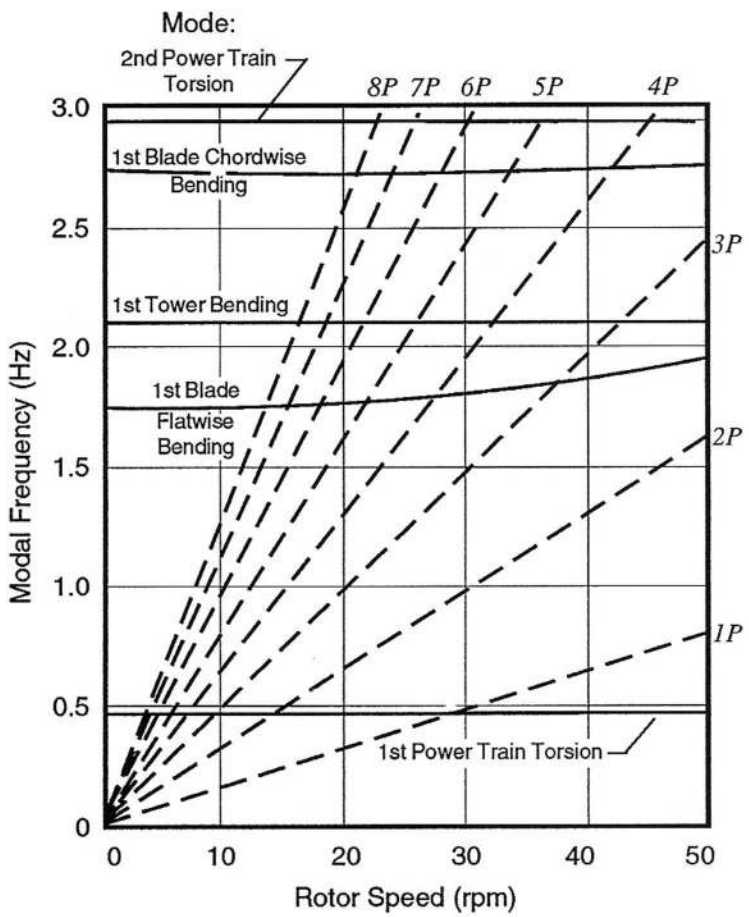

Figure 11-6. Typical Campbell diagram displaying the results of a HAWT modal analysis. Radial lines indicate the frequencies of potential excitation forces [Sullivan 1981]

Defining modal characteristics is of paramount importance in that, with this information, potentially harmful *resonant behavior* can be avoided. Resonance is a phenomenon which occurs in a structure when the frequency of periodic loading or *excitation* equals or nearly equals one of the modal frequencies of the structure. Thus, in Figure 11-6, every intersection of a radial line and a modal-frequency line is a potential resonance. Resonance if often characterized by a large increase in displacements and internal loads. The relative size of this increase is measured by a *dynamic amplification factor*, which is the ratio of the amplitude of the dynamic displacement to the static displacement under the same forcing function.

Not all resonances cause large amplification factors, because rotation can sometimes eliminate the matching of a forcing function with a natural mode, even when both have the same frequency in a non-rotating frame of reference. A general discussion of amplified and non-amplified resonances is beyond the scope of this chapter, but background information on resonances significant in HAWT systems is given in [Sullivan 1981].

In rotating structures, the acquisition of dynamic response characteristics is complicated by their dependence on the structure's rotational speed. Therefore, special methods have to be employed for both the predictive and experimental modal analysis. Predictive techniques for wind turbines are usually based on *the finite-element method*, in order to take advantage of its superior versatility. As the turbine is modeled in a frame of reference which rotates at the turbine operating speed (assumed constant), rotating coordinate system effects must be taken into account.

The finite-element method has been used extensively to predict the modal characteristics of rotating structures. When this method is applied to HAWT blades and other structures which are comprised of rotating beams reminiscent of fan or helicopter blades, some of the rotating coordinate system effects are neglected. This is usually justified when motions perpendicular to the axis of rotation (*i.e.*, along the axis of a HAWT blade) are relatively small. This is not the case for a VAWT, however, and these effects cannot be omitted. Here we will use a method similar to the one described by Patel and Seltzer [1971] for analyzing the modes of the spinning "Skylab" satellite, in which all rotating coordinate system effects are included.

Other analytical techniques which have been used to predict the dynamic characteristics of rotating structures include various *Galerkin* procedures [Klahs and Ginsberg 1979, Warmbrodt and Friedmann 1980], the *modal method*, and the *component mode method* in combination with various eigensolution schemes [Vollan and Zwaan 1977, Ottens and Zwaan 1978a and 1978b]. A major experimental obstacle to obtaining the natural frequencies and mode shapes of a rotating structure is that mechanisms must be devised for exciting the structure while it is rotating. Sliprings or telemetry must also be employed for data transmission from instruments such as *accelerometers* on the structure.

Finite Element Modal Analysis of a VAWT

When performing a modal analysis of a rotating structure, the motion is most conveniently measured relative to a coordinate system that is rotating with the structure. This permits the displacements to be small by eliminating the large rigid-body rotation. The coordinate system employed in this analysis rotates at the turbine operating speed, Ω, with the origin fixed in space at the lower bearing of the rotor. The angular velocity vector is directed vertically upward along the positive z axis. The finite-element matrices are developed on the basis of the motions that remain small within this rotating frame. For an accurate representation of the dynamics of a VAWT relative to a coordinate system rotating at a constant speed, the following effects must be included:

-- *tension stiffening*;
-- *centrifugal forces*;
-- *Coriolis accelerations.*

The tension stiffening that affects primarily the blades is induced by steady centrifugal and gravity forces. The centrifugal and Coriolis terms are a direct result of using a rotating coordinate system.

Equations of Motion

The total acceleration at a point in the rotating structure, with respect to fixed coordinates, can be represented in terms of the acceleration in the rotating coordinate system by an equation similar to Equation (11-18), as follows:

$$\boldsymbol{a}_t = \ddot{\boldsymbol{u}} + 2\Omega x \dot{\boldsymbol{u}} + \Omega x [\Omega x (\boldsymbol{r} + \boldsymbol{u})] \tag{11-41}$$

where

$\boldsymbol{a}_t$ = total acceleration vector, excluding gravity (m/s^2)
$\boldsymbol{r}$ = original position vector of an element; origin at lower bearing (m)
$\boldsymbol{u}$ = displacement vector; observed in the rotating coordinate system (m)
Ω = constant angular velocity vector of the rotating coordinate system (rad/s)

Using this expression for the acceleration in the *equation of motion* for a structure, the usual damping and stiffness matrices are altered from those of a static structure. The resulting differential equations are represented by

$$M\ddot{\boldsymbol{u}} + C\dot{\boldsymbol{u}} - S\boldsymbol{u} + K\boldsymbol{u} = \boldsymbol{F}_c + \boldsymbol{F}_g \tag{11-42}$$

where

M = normal (unaltered) mass matrix (kg)
u = displacement observed in the rotating coordinate system; dot signifies derivative with respect to time (m)
C = additional Coriolis matrix (N-s/m)
S = additional centrifugal softening matrix (N/m)
K = normal (unaltered) stiffness matrix (N/m)
F_c = additional static load vector representing steady centrifugal force (N)
F_g = gravitational forces; steady in a VAWT (N)

The Coriolis matrix, C, is *skew-symmetric* and results from the second term on the right side of Equation (11-41). Here we have ignored any structural (internal) damping because most VAWTs are lightly damped. Therefore, the $\boldsymbol{C}$ matrix is totally the result of Coriolis effects. The centrifugal softening matrix, S, comes from the variable portion (*i.e.*, dependent on $\boldsymbol{u}$) of the last term on the right in Equation (11-41). $\mathbf{F}_c$ also comes from the last term in Equation (11-41). To obtain the mode shapes and frequencies of the turbine as observed in the rotating system, Equation (11-41) is reduced to the following form:

$$M\ddot{\boldsymbol{u}} + C\dot{\boldsymbol{u}} + (K + K_G - S)\boldsymbol{u} = 0 \tag{11-43}$$

where K_G = geometric stiffness matrix resulting from steady centrifugal and gravitational loadings (N/m)

Thus, the solutions correspond to small motions about a prestressed state. *Aeroelastic* effects (*i.e.*, aerodynamic loading caused by structural motions) have not been included in this analysis. While strongly influencing the aerodynamic stability of a VAWT [*e.g.*, Popelka 1982], aeroelasticity seems to have little effect on the natural frequencies and modes of the turbine.

Eigenvalue Solution

Obtaining mode shapes and frequencies from Equation (11-43) involves solving what is known as a *characteristic-value problem*, which has the standard form

$$\begin{bmatrix} a_{11}x_1 + a_{12}x_2 + \cdots + a_{1n}x_n = \omega x_1 \\ a_{21}x_1 + a_{22}x_2 + \cdots + a_{2n}x_n = \omega x_2 \\ \cdots\cdots\cdots\cdots\cdots\cdots \\ a_{n1}x_1 + a_{n2}x_2 + \cdots + a_{nn}x_n = \omega x_n \end{bmatrix} \tag{11-44}$$

where, for our modal analysis problem

n = number of degrees of freedom; number of finite elements times three displacement components per element

$X_j \ldots x_n$ = *eigenvector* or *characteristic vector*; defines one mode shape

ω = *eigenvalue* or *characteristic value*; defines one modal frequency (rad/s)

Each non-trivial solution of this characteristic-value problem has an eigenvector and a corresponding eigenvalue, and the set of eigenvector/eigenvalue pairs comprises the results of a theoretical modal analysis of our structural system. Modes are usually presented in ascending order of frequency, from the lowest or *fundamental* mode to the highest frequency of interest. The latter seldom needs to exceed ten times the maximum rotational speed of the turbine ($10P$).

To find the eigenvalues of the system of equations represented by Equation (11-43), it is more convenient to use *state vectors* instead of the displacements u. Hence, we will introduce the state vector

$$\boldsymbol{v} = \begin{bmatrix} \dot{\boldsymbol{u}} \\ - - - \\ \boldsymbol{u} \end{bmatrix} \tag{11-45a}$$

and the matrices

$$\boldsymbol{A} = \begin{bmatrix} \boldsymbol{M} & 0 \\ - - & - - \\ 0 & \boldsymbol{K}' \end{bmatrix} \qquad \boldsymbol{B} = \begin{bmatrix} \boldsymbol{C} & \boldsymbol{K}' \\ - - & - - \\ -\boldsymbol{K}' & 0 \end{bmatrix} \tag{11-45b}$$

in which

$$\boldsymbol{K}' = \boldsymbol{K} + \boldsymbol{K}_G - \boldsymbol{S}$$

Equation (11-43) can now be written as

$$\boldsymbol{A}\dot{\boldsymbol{v}} + \boldsymbol{B}\boldsymbol{v} = 0 \tag{11-46}$$

Here $\boldsymbol{A}$ is *real symmetric*, and $\boldsymbol{B}$ is *real skew-symmetric.* Seeking a solution for Equation (11-46) in the form

$$\boldsymbol{v}(t) = \phi e^{i\omega t} \tag{11-47a}$$

where i is the square root of -1, the resulting eigenvalue problem is

$$[\boldsymbol{B} + i\omega\boldsymbol{A}]\phi = 0 \tag{11-47b}$$

We now define an eigenvector $\mathbf{x}$ as

$$\boldsymbol{x} = \boldsymbol{A}^{1/2}\phi \tag{11-47c}$$

assuming that $\boldsymbol{A}$ is now positive definite. We can now transform Equation (11-47b) into the standard eigenvalue form of Equation (11-44), with all terms on the left side, as follows:

$$[\boldsymbol{G} - \omega\boldsymbol{I}]\boldsymbol{x} = 0 \tag{11-48a}$$

$$\boldsymbol{G} = i\boldsymbol{A}^{-1/2}\boldsymbol{B}\boldsymbol{A}^{-1/2} \tag{11-48b}$$

Because of the skew-symmetry of the matrix $\boldsymbol{B}$, the matrix $\boldsymbol{G}$ is *Hermetian.* Consequently, it can be shown that the eigenvectors are, in general, complex; but the eigenvalues are real [Franklin 1968].[2] If structural damping is included, the system loses it Hermetian character and the eigenvalues as well as the eigenvectors are complex. Again, in the present analysis, structural damping has been ignored because VAWTs are lightly damped. The Hermetian character of the eigenvalue system has important ramifications to the rotating modal test. Even if the modes of the non-rotating structure are perfectly real, the modes of the rotating structure will be complex.

[2] If $\boldsymbol{A}$ is not positive-definite, then $\boldsymbol{G}$ is no longer Hermetian and the eigenvalues are not necessarily real. This condition can lead to dynamic instability.

NASTRAN Finite Element Modeling

The general-purpose structural analysis code *NASTRAN* is the software commonly used for modeling a wind turbine in finite elements to determine its natural vibration modes. Before presenting an example of the modeling, a short description of the NASTRAN calculational procedure is in order, as it is applied to this specific problem. Two of the available NASTRAN *rigid format* options are used in the modeling effort. First, a static analysis with geometric stiffening effects is performed on the model under the action of centrifugal, gravitational, and boundary forces. The resulting modified stiffness matrix ($K + K_G$ in Eq. (11-43)) is then retained *via* a modest amount of *DMAP* programming for use in the subsequent complex eigenvalue analysis (the second rigid format). Along with necessary structural data, the resulting data deck includes so-called "direct matrix input at grid points" (*DMIG*) cards. It is through these that the Coriolis and centrifugal softening matrices (C and S in Eq. (11-43)) are input to the model.

Because the required number of DMIG cards tends to be large, a pre-processor is generally used to make the inclusion of rotating coordinate system effects in NASTRAN relatively transparent to the user. This pre-processing program

-- reads the NASTRAN structural data deck and extracts needed information from *GRID, CBAR, MATI, CONM2*, and *RFORCE* cards;
-- constructs the necessary matrices and casts them in the DMIG card format;
-- inserts the DMIG data cards into the NASTRAN data deck.

NASTRAN users are provided with a choice of several complex eigensolvers. One employs the *upper-Hessenberg* method and is very efficient. A method that has been used successfully for the modal analysis of wind turbines is to first model the structure with the necessary number of degrees of freedom, then use a standard *Guyan reduction* procedure (also a NASTRAN option) to reduce the degrees of freedom to a manageable number (approximately 100) and then apply the upper-Hessenberg method.

Sample Theoretical Modal Analysis

In this sample modal analysis, taken from [Carne *et al.* 1982], modal shapes and frequencies are determined for the *Sandia/DOE 2-m VAWT* shown in Figure 11-7. The configuration of the finite-element model of this VAWT is shown in Figure 11-8. The model is composed of two blades, a central column, and elastic supports. The curved blades are modeled with 20 beam elements each. The truss column, which adds a fair degree of complexity to the model, is represented by 150 beam elements. The masses of the hardware associated with the upper bearing and its support-cable connections are represented by a single concentrated mass placed at the top of the truss model. The support cables are modeled with horizontal, linear springs and a vertical downward force on the truss, as shown in Figure 11-8.

The masses of the test instrumentation installed on the rotor (which are not negligible compared to the mass of the blades) are included by adding appropriate concentrated masses. The base structure is modeled as a concentrated mass in combination with torsional and linear springs. The horizontal springs at the upper and lower bearings have equal stiffnesses in two orthogonal directions, producing the desired isotropic boundary conditions typical of VAWTs. The stiffness and mass properties of the support system must usually be estimated, at least to some degree. The initial estimates for this model are given in parenthesis in the figure. The final properties of the supports were obtained by "tuning" the model to match frequencies measured when the VAWT was not rotating, as will be discussed in the next section.

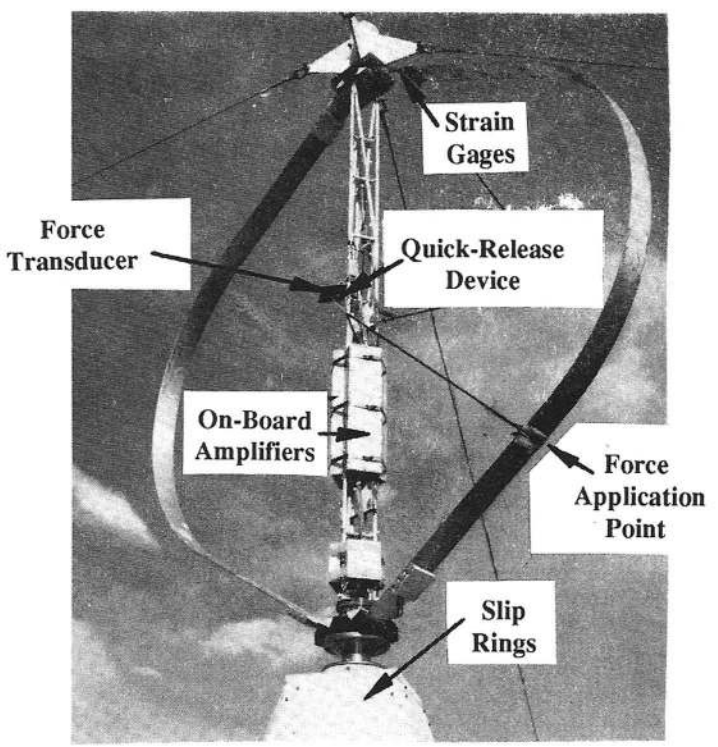

Figure 11-7. Sandia/DOE 2-m test VAWT with typical modal-survey instrumentation and excitation devices. (*Courtesy of Sandia National Laboratories*)

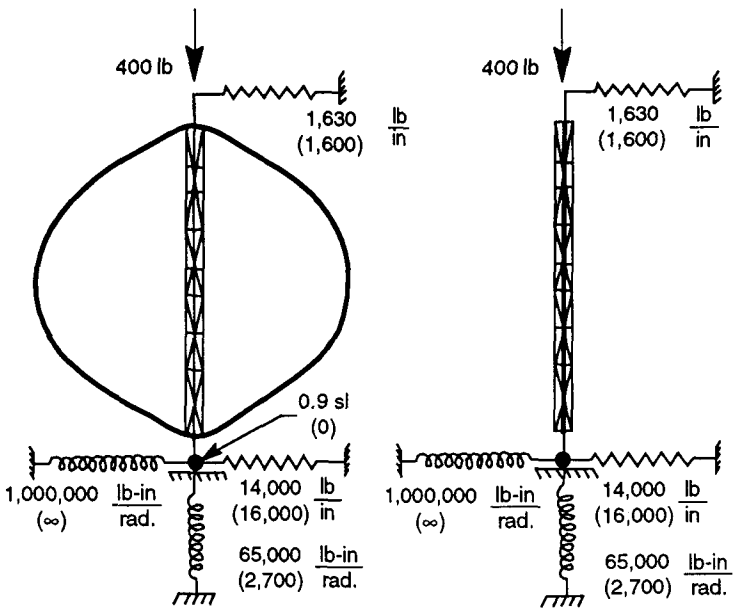

Figure 11-8. Finite-element model of the 2-m VAWT. [Carne *et al.* 1982]

Non-Rotating System Modes

Table 11-1 lists the frequencies of the first ten modes of vibration on the non-rotating (*i.e.*, parked) 2-m VAWT, with its rotor brake on. The first column gives the mode number, usually assigned in increasing order of frequency. Mode identification terminology is given in the second column. The corresponding mode shapes, in three views, are sketched in [Carne *et al.* 1982]. The third column lists the frequencies measured with the rotor parked, and the fourth column gives the frequencies calculated using initial estimates of the support mass and stiffness properties. Again, these estimates are the data in parenthesis in Figure 11-8. In the fifth column of Table 11-1 are the "tuned" calculations of the modal frequencies for the non-operating condition. The last column in the table gives the relative changes in frequency resulting from tuning the model.

Tuning the Finite-Element Model

The differences between the initial and tuned frequencies, ranging from -20% to +8%, indicate the scale of the errors that can be present when (1) the support system and the resulting theoretical boundary conditions are complicated, and (2) some of the auxiliary components in the structural system are not modeled in detail. For practical reasons, the latter is usually the case. As a result, a finite-element model must be calibrated against a basic set of measured responses, on the same or a similar structure, to establish confidence in predictions made with it of natural frequencies under operating conditions. Modal analysis is clearly recognized to be a combination of theoretical and experimental methods.

Table 11-1.
Modal Frequencies of the Non-Rotating 2-m VAWT [Carne *et al.* 1982]

Mode Number	Mode name	Test (Hz)	Initial model (Hz)	Tuned model (Hz)	Tuning change (Hz)
1	1st Anti-Symmetric Flatwise	12.3	12.5	12.3	-1.6%
2	1st Symmetric Flatwise	12.5	12.6	12.4	-1.6%
3	1st Rotor Out-of-Plane	15.3	17.1	15.2	-11.1%
4	1st Rotor In-Plane	15.8	17.2	15.9	-7.6%
5	Dumbbell	24.4	22.6	24.4	+8.0%
6	2nd Rotor Out-of-Plane	26.2	30.5	26.2	-14.1%
7	2nd Rotor In-Plane	28.3	30.6	28.0	-8.5%
8	2nd Symmetric Flatwise	29.7	30.9	30.6	-1.0%
9	2nd Anti-Symmetric Flatwise	31.5	39.7	31.7	-20.2%
10	3rd Rotor Out-of-Plane	36.5	42.3	36.5	-13.7%

Calculated Rotating System Modes

The Campbell diagram in Figure 11-9 presents the modal frequencies of the 2-m VAWT at rotor speeds from 0 to 600 rpm. The curves in this figure are the calculated frequencies obtained using the tuned NASTRAN model, with mode numbers corresponding to those in Table 11-1. The variations of the frequencies with rotor speed are quite complex. While most increase monotonically with speed, some decrease monotonically. Others increase and then decrease and *vice versa.* These variations are similar to those associated with the classical whirling-shaft problem. In addition to complicated frequency variations, the mode shapes also change in character with rotor speed. Specifically, mode shapes which are completely *uncoupled* when the turbine is parked become coupled during rotation. This coupling is discussed in more detail in [Carne *et al.* 1982]. In mathematical terms, the modes change from real to complex as the turbine rotates.

Sample Experimental Modal Analysis

An overview of the general techniques for modal testing of wind turbines will now be presented, again using the Sandia/DOE 2-m VAWT as an example. Portable data acquisition tools of the test engineer are based on *the fast Fourier transform.* The FFT technique, which involves exciting the structure with a force having a linear spectrum containing the frequency band of interest, is generally faster and more versatile than the classical *swept-sine* technique. The applied forces and responses are measured in the time domain and transformed to the frequency domain using the FFT. The frequency response functions are then computed from the cross-spectral and auto-spectral densities of the applied force and the responses.

Typically, several measurements are averaged to reduce the effects of uncorrelated noise. A more-complete description of FFT modal testing is contained in [Klosterman and Zimmerman 1975]. The greater versatility of this technique is a result of its more-relaxed requirements on the excitation force. For example, the FFT technique is equally applicable to shaker-driven excitations, instrumented-hammer impacts, and excitations by wind forces.

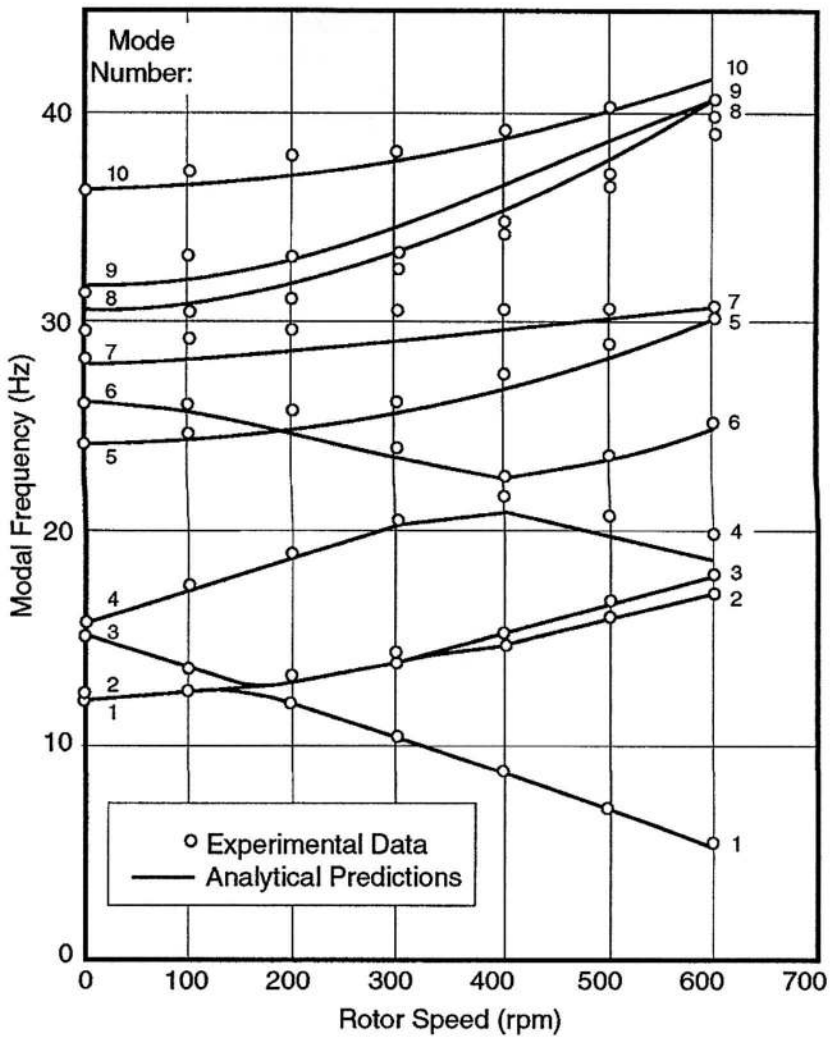

Figure 11-9. Campbell diagram of the Sandia/DOE 2-m VAWT, presenting both theoretical and experimental modal frequencies *vs.* rotor speed. [Carne *et al.*, 1982]

Instrumentation

The general layout of instrumentation on the test VAWT is illustrated in Figure 11-7. For non-rotating tests, the turbine was instrumented with 18 piezoelectric accelerometers on the blades, 10 on the central column, 20 on the supporting pedestal, and 6 on the turbine shaft assembly. All input and response signals were low-passed at 100 Hz, amplified as necessary with signal-conditioning amplifiers, and recorded on a 14-channel tape recorder. In the rotating modal test the high, steady centrifugal accelerations prevented the use of accelerometers except on the central column. Strain gages are normally installed on newly-designed wind turbines undergoing development tests, and these gages are commonly used as response transducers for modal tests as well.

For this rotating test, strain gages were placed on the blades and central column, using a double-active gage in the bridge so that bending about a single axis would be measured. Gages were placed near the blade roots on leading and trailing edges (to measure chordwise bending), on the inside and outside surfaces at maximum blade thickness (to measure flat-wise bending), and on the central column (to measure in-plane and out-of-plane bending). On-board amplifiers boosted the strain signal to 2,000 psi/V for all gages, in order to give an adequate level for passing through the sliprings and the long wires that are typically required for modal tests on operating wind turbines. Because of expected difficulties in understanding the modes of the rotating central column, two piezoresistive accelerometers were attached to the upper column to record in- and out-of-plane motions.

Excitation

The scope of methods used to excite vibrations in wind turbines for modal analysis is broad. These methods fall into the four general categories of human, impact, step-relaxation, and natural-wind. As mentioned previously, the FFT-testing procedure allows flexibility in the excitation method, which is of significant benefit.

Human

Human excitation is the simplest approach to implement, but has the most limitations. The large displacement, low frequency modes of large wind turbines allow a test engineer to manually input a quasi-sinusoidal force into the structure to excite a single mode of the system. The frequency and damping parameters of the mode can be determined as the systems rings down after the excitation is removed. This approach was used to test over 20 commercial 17-m VAWTs in as little as 1¼ hours each. This study also provided valuable insight into the structural-dynamic variability of duplicate units in the field [Lauffer, 1986].

Impact

Impact excitation methods range from using an instrumented 3-lb hammer to strike the 2-m VAWT at various locations on its blades and central tower to swinging a 1,000-lb ram from a crane to strike the tip of the NASA/DOE 2.5-MW Mod-2 HAWT [Boeing 1982]. In both cases, the impact force must be of sufficient amplitude and duration to excite the modes and frequencies of interest. This is accomplished by prior calibration tests.

Impact testing was also one of the techniques used to test the Sandia 34-m VAWT Test Bed in various stages of assembly. This allowed model correlation of substructure models before final model assembly. The substructures tested included two blade sections and a blade assembly. Step-relaxation and natural wind excitation were also used for other substructures, as appropriate [Carne *et al.*, 1989].

Impact testing was also used to study the use of a Laser Doppler Velocimeter (LDV) for non-contact measurements of a HAWT in the field. This study used impact excitation to compare the LDV to traditional accelerometers as well as to study damage detection techniques. A comparison to natural wind excitation was also performed. The test object in this study, a 15 m diameter HAWT in its parked configuration [Rumsey *et al.*, 1997].

Step-Relaxation

Step-relaxation relies of the quick release of strain energy in a pretensioned cable for the excitation of the structure. A small device applying a force of approximately 50 lb was used successfully on the 2-m VAWT [Carne *et al.* 1982]. A heated wire was used to burn through a nylon cord to affect the quick release of the excitation force. For a modal test of the 64-m diameter *Eolé* (Fig. 3-38) two separate force-application points were used, one on the central column and one on a blade [Carne *et al.* 1988]. Forces were applied through high-strength steel cables loaded with a diesel-powered winch and restrained by a nylon strap. Loads of 135 kN (30,000 lb) and 45 kN (10,000 lb) were applied to the column and blade, respectively.

One difficulty in using step relaxation is related to the FFT algorithm. A quick release basically applies a force which is a *Heaviside* function, for which there is no Fourier transform. However, if the Heaviside function is passed through a high-pass filter, it can be converted to a well-behaved function that is easily transformable with the FFT.

Natural Wind

Using the natural wind to excite the turbine has certain advantages, as discussed in [Carne *et al.* 1988]. Two of the most significant are the greatly reduced cost and complexity of the test and the ability to test during windy conditions. Wind-excitation methods were developed during test of the Eolé VAWT, and these produced modal frequencies in excellent agreement with those obtained by step relaxation. However, damping information is not as readily available from the power spectra obtained using wind excitation. Development of the Natural Excitation Technique (NExT) rectified this situation and will be discussed below [James *et al.*, 1995].

Measured Rotating System Modes of the 2-m VAWT

The results of the modal testing performed on the 2-m VAWT using step-relaxation excitation are shown by the data points in Figure 11-9. The correlation here is typical of wind turbine modal analysis. The average absolute deviation of the experimental frequencies from the theoretical (tuned-model) frequencies is 0.5 Hz, or 2.2%. Deviations generally increase with increasing rotor speed, which is a characteristic of finite-element models that do not have a sufficient number of degrees of freedom to accurately represent complex mode shapes.

Development of Natural Wind Excitation Testing

The structural dynamics of rotating VAWT machines are critical design conditions that require experimental techniques that can match the fidelity of the advanced analyses described previously. The previous example using the 2-m VAWT showed the power of performing step-relaxation testing during rotation. However, this approach is technically intensive and would not be generally applicable for many operational scenarios. As mentioned previously, the use of natural wind excitation is a more generally applicable approach and allows testing in the actual operating environment. This section details the development of the natural excitation technology in the form of the *natural excitation technique* or NExT [James *et al.*, 1995]. A more complete background on the historical development of the natural wind excitation testing for wind turbines is also available [Carne and James 2008].

Theoretical Development of NExT

A critical step in the development of NExT was to find a relationship between modal parameters of structural interest (such as frequency and damping) and a function that could be produced from measured response data. For NExT, the *cross-correlation function* between two response–only measurements was used. The derivation of the relationship of modal parameters and the cross-correlation function begins by assuming the standard matrix equations of motion:

$$[M]\{\ddot{x}(t)\} + [C]\{\dot{x}(t)\} + [K]\{x(t)\} = \{f(t)\} \tag{11-49}$$

where

$[M]$ = mass matrix (g)
$[C]$ = damping matrix(N-s/m)
$[K]$ = stiffness matrix (N/m]
$\{f\}$ = vector of random forcing functions (N)
$\{x\}$ = vector of random displacements (m)
t = elapsed time (s)
$\dot{x}, \ddot{x}$ = first and second derivatives with respect to time (m/s, m/s^2)

Equation (11-49) can be expressed in modal coordinates using a standard modal transformation after performing a standard matrix diagonalization (assuming proportional damping). A solution to the resulting scalar modal equations can be obtained by means of a Duhamel integral, assuming a general forcing function, $\{f\}$, with zero initial conditions (*i.e.* zero initial displacement and zero initial velocity). The solution equations can be converted back into physical coordinates and specialized for a single input force and a single output displacement using appropriate mode shape matrix entries. The following equations result:

$$x_{ik}(t) = \sum_{r=1}^{n} \psi_{ir}\psi_{kr} \cdot \int_{-\infty}^{t} f_k(\tau) g^r(t-\tau) d\tau \tag{11-50}$$

$$g^r(t) = 0, \quad for \ t < 0$$

$$g^r(t) = \frac{1}{m^r \omega_d^r} \exp\left(-\zeta^r \omega_n^r t\right) \sin\left(\omega_n^r t\right), \quad for \ t \geq 0;$$

where

ω_d^r = $\omega_n^r (1 - \zeta^{r2})^{1/2}$ is the damped modal frequency (rad/s)
ω = *rth* modal frequency (rad/s)

ζ^r = *rth* modal damping ratio
m^r = *rth* modal mass (g)
n = number of modes;
ψ_{ir} = *ith* component of mode shape r

The next step of the theoretical development is to form the cross-correlation function of two responses (x_{ik} and x_{jk}) to a white noise input at a particular input point *k*. The cross-correlation function $\Re_{ijk}(T)$ can be defined as the expected value of the product of two responses evaluated at a time separation of *T*:

$$\Re_{ijk}(T) = E[x_{ik}(t+T)\, x_{jk}(t)] \tag{11-51}$$

where *E* is the *expectation operator.*

Substituting Equation (11-50) into (11-51), recognizing that $f_k(t)$ is the only random variable, allows the expectation operator to depend only on the forcing function. Using the definition of the *autocorrelation function*, and assuming for simplicity that the forcing function is white noise, the expectation operation collapses to a scalar times a *Dirac delta function.* The Dirac delta function then collapses one of the Duhamel integrations embedded in the cross-correlation function. The resulting equation can be simplified via a change of variable of integration, setting $\lambda = t\text{-}\tau$. Using the definition of *g* from Equation (11-50) and the trigonometric identity for the sine of a sum results in all the terms involving *T* being separated from those involving λ. This separation allows terms that depend on *T* to be factored out of the remaining integral and out of one of the modal summations, with the following results:

$$\Re_{ijk}(T) = \sum_{r=1}^{n} \begin{bmatrix} A^r_{ijk} \exp\left(-\zeta^r \omega_n^r T\right) \cos\left(\omega_d^r T\right) \\ + B^r_{ijk} \exp\left(-\zeta^r \omega_n^r T\right) \sin\left(\omega_d^r T\right) \end{bmatrix} \tag{11-52}$$

where A^r_{ijk} *and* B^r_{ijk} are independent of *T*, are functions of only the modal parameters, and completely contain the remaining modal summation, as shown in the following equations:

$$\begin{Bmatrix} A^r_{ijk} \\ B^r_{ijk} \end{Bmatrix} = \sum_{s=1}^{n} \frac{\alpha k \psi_{ir}\psi_{kr}\psi_{js}\psi_{ks}}{m^r \omega_d^r\, m^s \psi_d^s} \cdot \int_0^{\infty} \exp\begin{pmatrix} -\zeta^r \omega_n^r \\ -\zeta^s \omega_n^s \end{pmatrix} \lambda \cdot \sin\left(\omega_d^s \lambda\right) \begin{Bmatrix} \sin\left(\omega_d^r \lambda\right) \\ \cos\left(\omega_d^r \lambda\right) \end{Bmatrix} d\lambda. \tag{11-53}$$

Equation (11-52) is the key result of this derivation. Examining Equation (11-52), the cross-correlation function is seen to be a sum of decaying sinusoids, with the same characteristics as the impulse response function of the original system. Thus, cross-correlation functions can be used as impulse response functions in time-domain modal parameter estimation schemes. This is more clearly seen after further simplification using a new constant multiplier (Gj^r), as follows:

$$R_{ij}(T) = \sum_{r=1}^{n} \frac{\psi_{ir} G_j^r}{m^r \omega_d^r} \exp\left(-\zeta^r \omega_n^r T\right) \sin\left(\omega_d^r T + \Theta r\right). \tag{11-54}$$

James *et al.* [1995] present more definition of the intermediate steps in this derivation and the results of analytical verification checks of the derivation.

Comparison of NExT Test Data from a Rotating VAWT to Simulated Data

An interesting comparison was performed between NExT data processing results and simulated data and using the known modal parameters. For this activity, a simulation code (VAWT-SDS), was used to compute the time domain response of the DOE/Sandia 34-m VAWT test bed (Figure 2-2) during rotation in turbulent wind [Dohrmann and Veers, 1989]. The structural model (including rotational effects) used in VAWT-SDS was available to calculate the analytical modal frequencies and analytical modal damping. VAWT-SDS was used to generate analytical data, which were then input to NExT. The results were compared to the known frequencies and damping information to test the capabilities of NExT.

Simulated data were generated for the 34-m testbed using a 30 rpm rotation rate and 20 mph (8.9 m/s) turbulent winds with 15% turbulence intensity. Stiffness proportional damping, sufficient to produce a damping ratio of 0.2% at 1.4 Hz was added to the model. Time histories of 2,048 points for eight strain gauge outputs were generated using a step size of 0.04 s. Sensor noise was simulated by adding a white-noise signal to each simulated time history. The standard deviation of this additive signal was 2% of the standard deviation of each time history. The analytical modal frequencies and damping ratios were also calculated by extracting the complex eigenvalues from the structural matrices used in the VAWT-SDS code. VAWT-SDS used the Newmark-Beta numerical integration scheme, and the approximations inherent in this procedure produced period elongations. The frequency shifts created by numerical integration were calculated and a correction was added to the analytical values [James *et al.*, 1996].

NExT was used to estimate modal frequencies and damping ratios from the simulated data so that the NExT results and the analytical values could be compared. Table 11-2 shows the results of the comparison. With NExT, it was possible to correctly extract the frequencies and damping from the data with the exception of the first two modes at 1.27 Hz and 1.35 Hz. These two modes are very closely spaced, making it difficult to obtain accurate frequen-

Table 11-2.
Comparison of NExT With Simulated Results [James *et al.*, 1993]

Mode	Frequency (Hz)		Damping (%)	
	Simulated	NExT	Simulated	NExT
1st Flatwise Antisymmetric	1.27	1.31	0.2	0.4
1st Flatwise Symmetric	1.35	1.32	0.2	0.3
1st Blade Edgewise	1.59	1.59	0.3	0.3
1st Tower In-Plane	2.02	2.01	0.3	0.4
2nd Flatwise Symmetric	2.43	2.44	0.4	0.5
2nd Flatwise Antisymmetric	2.50	2.50	0.4	0.4
1st Tower Out-of-Plane	2.80	2.80	0.3	0.5
2nd Rotor Twist	3.39	3.39	0.5	0.6
2nd Tower In-Plane	3.46	3.45	0.5	0.4
3rd Flatwise Antisymmetric	3.65	3.63	0.5	0.4
3rd Flatwise Symmetric	3.73	3.73	0.6	0.4
2nd Blade Edgewise	3.88	3.87	0.5	0.3

cy or damping results from NExT. It should also be noted that the higher modes (3.65 Hz, 3.73 Hz, and 3.88 Hz) have NExT-estimated damping ratios that are lower than the specified damping ratios. The amplitudes of these modes are low compared to the noise level, which affected the estimates. This finding suggested the need for longer time histories to improve the accuracy. Also, this comparison shows the validity of natural wind excitation as a tool for wind turbine testing, as well as pointing out the issues (such as period elongations) associated with numerical integration schemes used in analysis codes.

Comparison of NExT to Non-Rotating Step Relaxation Excitation

Another insightful comparison is between NExT processing using wind excitation and traditional analysis using step-relaxation excitation. For this comparison, a FloWind Corporation 19-m VAWT in Altamont Pass, CA, was tested using step-relaxation modal testing techniques during quiescent daytime winds. NExT was then used during periods of more substantial nighttime winds (above 7 m/s or 16 mph). The turbine was parked (nonrotating) during all testing. Accelerometers were used to measure the response at predetermined locations on the turbine. This allowed a comparison between modal parameters estimated by NExT and modal parameters estimated using conventional testing techniques (step-relaxation testing).

Table 11-3 compares the modal frequencies and modal damping ratios of the 19-m VAWT as determined from conventional testing and from NExT. The two methods produced estimates of the modal frequencies that are in good agreement, particularly in view of the temperature difference between day and night. The average difference for the ten modes is only 0.5%. Also, the modal damping ratios of all six of the tower modes (rotor twist, tower in-plane, tower out-of-plane) are very similar. However, the modal damping ratios of all four blade flatwise modes (flatwise symmetric and flatwise antisymmetric) are substantially higher from NExT estimates.

Table 11-3.
Comparison of NExT With Step-Relaxation Excitation [James *et al.*, 1993]

Mode	Frequency (Hz)		Damping (%)	
	Step Relax	NExT	Step Relax	NExT
1st Rotor Twist	2.37	2.38	0.2	0.1
1st Flatwise Antisymmetric	2.48	2.49	0.2	1.3
1st Flatwise Symmetric	2.51	2.51	0.1	1.4
1st Tower Out-of-Plane	2.72	2.76	0.4	0.4
1st Tower In-Plane	3.11	3.15	0.4	0.4
2nd Tower Out-of-Plane	4.53	4.53	0.1	0.1
2nd Flatwise Antisymmetric	5.30	5.31	0.3	0.8
2nd Flatwise Symmetric	5.64	5.65	0.1	0.6
2nd Rotor Twist	6.59	6.62	0.1	0.1
2nd Tower In-Plane	6.64	6.71	0.3	0.6

Subsequent analysis suggested that these differences were due to a drag phenomenon experienced as the largest cross-section of the blade oscillated normal to the stronger nighttime winds [James *et al.*, 1995]. This exercise showed the utility of performing modal testing in an operating environment to allow the extraction of the total damping (structural and aeroelastic). This test series also pointed out the reduced infrastructure associated with the natural excitation test while clarifying the utility of traditional testing to separate out the different physical phenomena acting on wind turbine structures.

Application of NExT to a Rotating VAWT

The significant utility of wind excitation is the ability to extract structural dynamics information from a rotating system. NExT was used to extract modal frequency and damping using data from the DOE/Sandia 34-m testbed during rotation at 0, 10, 15, 20, 28, 34, and 38 rpm. The wind speed during these tests was also approximately 10 m/s (22 mph). Twelve strain gauges (accessed through slip rings) were used as the sensors in all of these analyses. Time history length, sample rate, correlation block size, and the time domain analysis parameters were all the same as provided in the previous section. Figure 11-10 is a plot of the rotation-rate dependent modal frequencies of this turbine from analysis and from experiment using NExT.

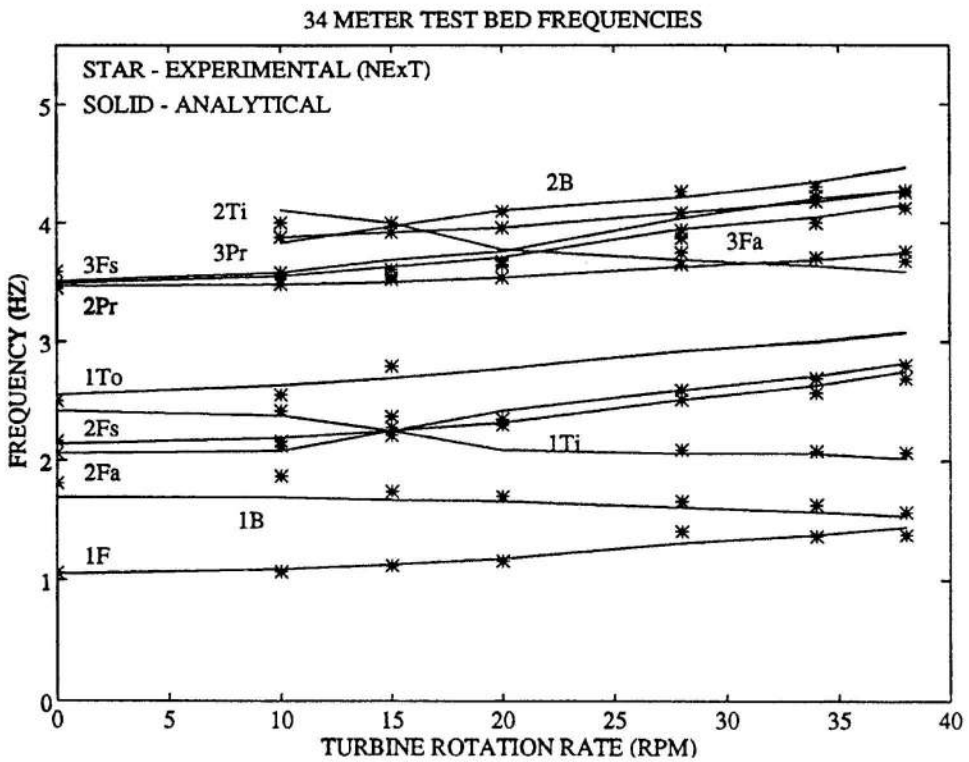

Figure 11-10. Modal frequencies versus rotor rotation rate for the Sandia/DOE 34-m VAWT. [James *et al.*, 1993]

Figure 11-11 shows a plot of modal damping ratios, as calculated with NExT, versus turbine rotation rate for the blade flatwise modes. The damping ratios of these modes generally increase significantly with turbine rotation rate. For example, the first flatwise damping ratio increases from 2% to 7%. The notable exception is the second blade flatwise mode that drops between 15 rpm and 28 rpm. Such a drop in damping ratio is likely due to modal coupling to a more lightly damped mode, since modal coupling varies with rotation speed. This data validates the need to understand the variation in parameters in operating conditions including rotation rate effects, especially in variable-speed machines or during start-up/ shut-down.

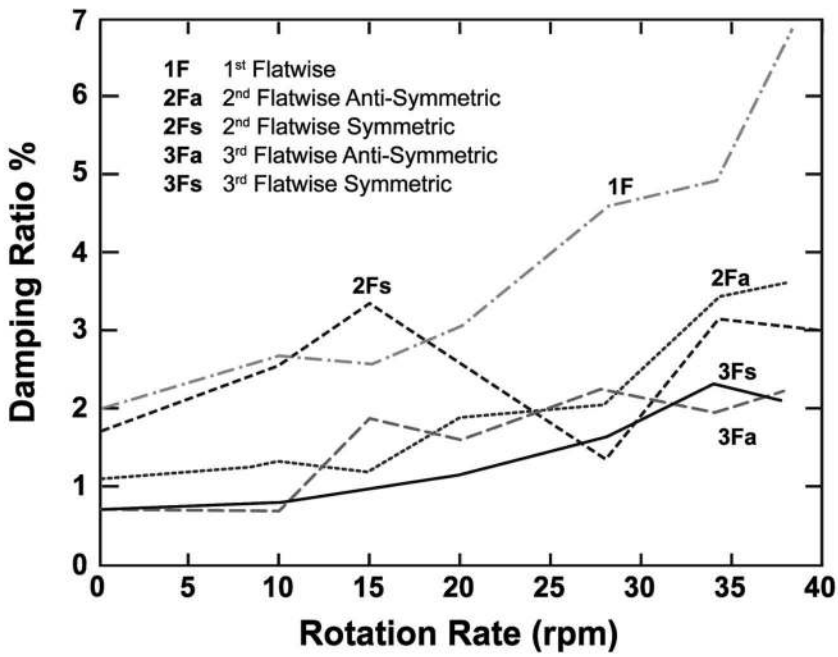

Figure 11-11. Modal damping versus rotor rotation rate for the Sandia/DOE 34-m VAWT. [James *et al.*, 1993]

Application of NExT to HAWT Systems

Table 11-4 shows the results of comparison between impact excitation and natural excitation on a parked HAWT. In this case the machine was an Atlantic Orient Corporation (AOC) 15/50, which is a three-bladed turbine with a 15-m rotor mounted downwind of the tower. The results show a very close agreement between the measured frequencies and a typical agreement for the damping values [Rumsey *et al.*, 1997].

A controlled yaw or upwind-rotor HAWT is the most direct application of NExT to a rotating turbine, as the kinematics of the system are primarily limited to rotation of the blades. This class of turbine shows the same dynamic characteristics as the rotating VAWT, including distinct natural frequencies, environment-dependent damping, and rotation-dependent forced harmonics. NExT has been applied to field results from a Northern Power Systems 100-kW HAWT, which has a two-bladed teetering rotor, 17.8 m in diameter [James, 1994]. Figure 11-12 displays some representative data from this analysis. In this case the damping in the 5.34 Hz edgewise mode is plotted versus wind speed. The damping is seen to have a clear and increasing trend as the wind speed increases.

Table 11-4.
Comparison of Two Modes from a Parked AOC 15/50 HAWT Using NExT and Impact Excitation [Rumsey *et al.*, 1997]

Mode	Frequency (Hz)		Damping (%)	
	Impact	NExT	Impact	NExT
Teeter	3.19	3.18	1.18	1.58
Umbrella	3.72	3.73	1.11	1.27

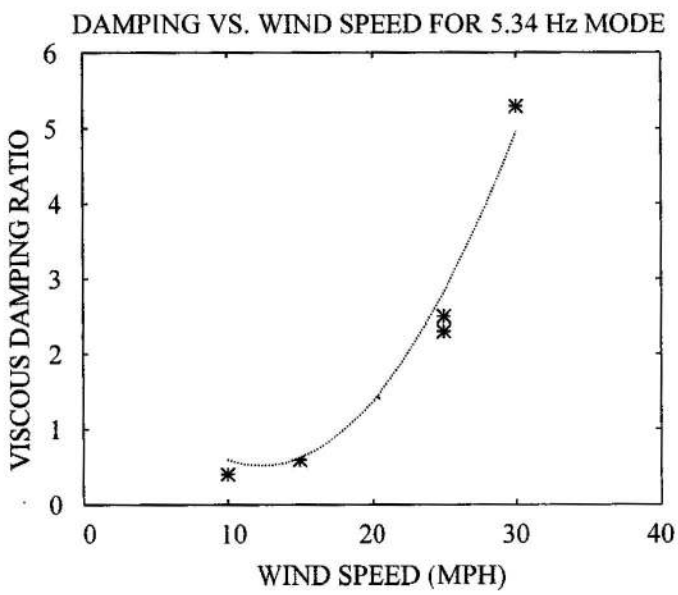

Figure 11-12. Damping versus wind speed for the 5.34 Hz edgewise mode of the Northern Power Systems 100-kW HAWT. [James, 1994]

A more challenging dynamical system is a free-yaw HAWT with its rotor mounted downwind of the tower. This turbine configuration can be simpler to build, but the uncontrolled yaw degree-of-freedom couples to the other in-plane dynamic modes and creates entire families of frequency-dependent phenomena. Figure 11-13 shows an example from the free-yaw 26-m diameter Advanced Wind Turbines AWT-26, which is a downwind teetering-rotor machine [Malcolm and James 1995]. The expected per-rev harmonic forcing function frequencies are plotted as the dotted lines. The solid lines denote the analytically-predicted natural frequency families. These frequencies are only distinct in the non-rotating condition.

As the machine rotates, natural frequencies split into multiple rotation-rate dependent frequencies. NExT was used to process field data from this HAWT as it was rotating at 58 rpm. There is a slight mismatch between the analysis and the field test data. This mismatch illustrates the utility of extracting structural dynamics data from an operating machine for comparisons to analytical data.

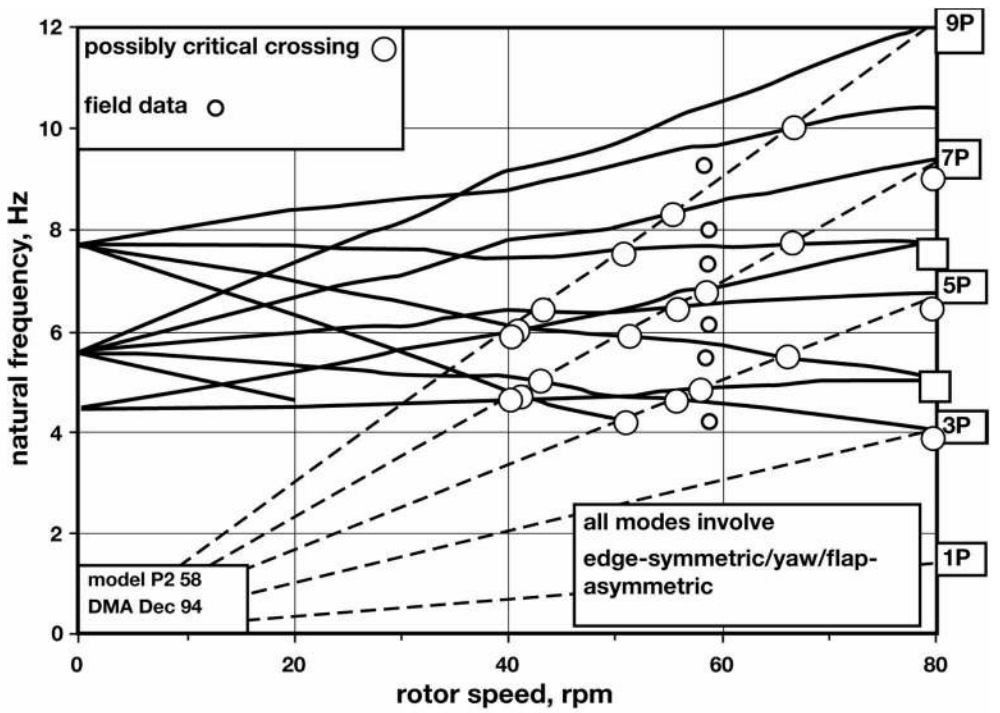

Figure 11-13. Periodic natural frequency families including NExT-derived field data *vs.* rotor speed for the AWT-26 HAWT. [Malcolm and James, 1995]

Classical Aeroelastic Flutter Analysis for HAWTs

Background

Flutter is a self-starting and potentially destructive vibration where aerodynamic forces on an object couple with a structure's *natural mode of vibration* to produce rapid *periodic motion*. Flutter can occur in any object within a strong fluid flow, under the conditions that a *positive feedback* occurs between the structure's natural vibration and the aerodynamic forces. That is, when the vibrational movement of an object like a flexible airfoil increases an aerodynamic load which in turn drives the object to move further. If the energy during the period of aerodynamic excitation is larger than the natural *damping* of the system, the level of vibration will increase. The vibration levels can thus build up and are only limited when the aerodynamic or mechanical damping of the object match the energy input. This often results in large amplitudes and can lead to rapid failure.

Although classical aeroelastic flutter has generally not been a driving issue in utility-scale wind turbine design, one case in which classical flutter was observed involved a vertical-axis wind turbine (VAWT) turning in still air [Popelka 1982]. The rotor was purposefully motored at ever-increasing speeds until the flutter boundary was breached and dramatic classical flutter oscillations were observed. Flutter occurred at approximately twice the design operating speed of the rotor.

For very large horizontal-axis wind turbines (HAWTs) fitted with relatively soft (flexible) blades, classical flutter becomes a more important design consideration. Innovative blade designs involving the use of *aeroelastic tailoring*, wherein the blade twists as it bends under the action of aerodynamic loads to shed loads resulting from wind turbulence, increase the blades proclivity for flutter.

Analytical Model of Flutter

The analysis of classical flutter in wind turbines necessitates the use of unsteady aerodynamics. As pointed out by Leishman [2002], for horizontal axis wind turbines there are two interconnected sources of unsteady aerodynamics. The first is a result of the *trailing wake* of the rotor and is addressed by investigating the interactions between the rotor motion and the inflow. The second, which will be the focus here, is due to the *shed wake* of the individual blades and can be addressed using techniques developed for analyzing flutter in fixed-wing aircraft.

To simplify the analysis, the rotor is assumed to be turning in still air. Because there is no wind inflow, unsteady aerodynamics caused by the trailing wake can be neglected. Consequently, the aerodynamic behavior of a single blade is similar to that of a fixed wing with a free stream velocity that varies linearly from the root to the tip, assuming that the shed wake of the preceding blade dies out sufficiently fast so that the oncoming blade will encounter essentially still air on a hub fixed in space. Focusing on aeroelastic stability associated with the shed wake from an individual HAWT blade, the technique developed by Theodorsen [Theodorsen 1935, Fung 1969, Dowell 1995] for fixed wing aircraft has been adapted for use with HAWT blade flutter [Lobitz 2004].

The Theodorsen technique specifically addresses classical flutter in an infinite *(i.e.* two dimensional with no end effects) airfoil undergoing oscillatory pitching and plunging motion in an incompressible flow, as illustrated in Figure 11-14. The airfoil's pitching motion is represented by the angle α and its plunging motion by the vertical translation h. L represents the lift force vector positioned at the quarter-chord, M is the pitching moment about the *elastic*

axis and *U* is the free-stream wind velocity. The origin of the coordinate system is positioned along the chordline at the section elastic axis. Note that *a* is defined as the fraction of *b* (the half-chord) that the elastic axis is aft of the mid-chord. Thus in Figure 11-14, *a* is negative since the elastic axis is ahead of the mid-chord.

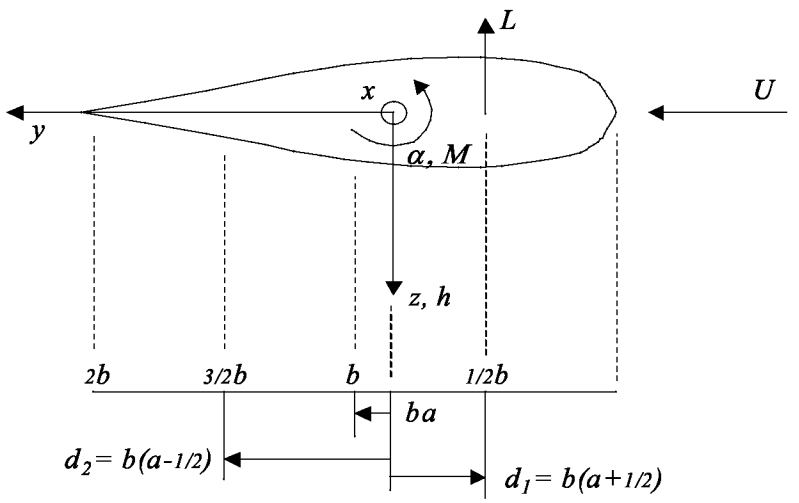

Figure 11-14. Schematic diagram of motions of a blade cross section assumed in the application of the Theodorsen technique for analyzing the flutter of a fixed wing and adapted for wind turbine blades.

The blade is assumed to be simultaneously pitching and plunging in an oscillatory fashion at a modal natural frequency ω, as follows:

$$h = h_0 e^{i\omega t} \quad \text{and} \quad \alpha = \alpha_0 e^{i\omega t} \tag{11-55}$$

Q5

where

h = vertical displacement (m)
h_0 = complex constant (m)
ω = modal natural frequency (rad/s)
t = elapsed time (s)
α = pitch angular displacement (rad)
α_0 = complex constant (rad)

According to the Theodorsen model, the lift force, *L*, and the pitching moment, *M*, are given by Equations (11-56), where *a*, *b*, d_1, and d_2 are as shown in Figure 11-14.

$$L = 2\pi\rho U^2 b \left\{ \begin{array}{l} \dfrac{i\omega C(k)}{U} h_0 + C(k)\alpha_0 + [1 + C(k)(1-2a)]\dfrac{i\omega b}{2U}\alpha_0 \\ -\dfrac{\omega^2 b}{2U^2} h_0 + \dfrac{\omega^2 b^2 a}{2U^2}\alpha_0 \end{array} \right\} \tag{11-56a}$$

$$M = 2\pi\rho U^2 b \left\{ \begin{array}{l} d_1 \left[\frac{i\omega C(k)}{U} h_0 + C(k)\alpha_0 + [1 + C(k)(1 - 2a)] \frac{i\omega b}{2U} \alpha_0 \right] + d_2 \frac{i\omega b}{2U} \alpha_0 \\ - \frac{\omega^2 a b^2}{2U^2} h_0 + \left(\frac{1}{8} + a^2 \right) \frac{\omega^2 b^3}{2U^2} \alpha_0 \end{array} \right\} \tag{11-56b}$$

where

L = lift force intensity; force per unit length of span (N/m)
M = pitch moment intensity, moment per unit length of span (N-m/m)
U = resultant airspeed (m/s)
$C(k)$ = complex-valued Theodorsen function
k = reduced frequency (rad)

The Theodorsen function, $C(k)$ and the reduced frequency, k, are defined as follows:

$$k = \omega b/U \tag{11-57a}$$

$$C(k) = \frac{H_1^{(2)}(k)}{H_1^{(2)}(k) + iH_0^{(2)}(k)} \tag{11-57b}$$

where H denotes the Hankel function. The real and imaginary parts of C are displayed graphically in Figure 11-15.

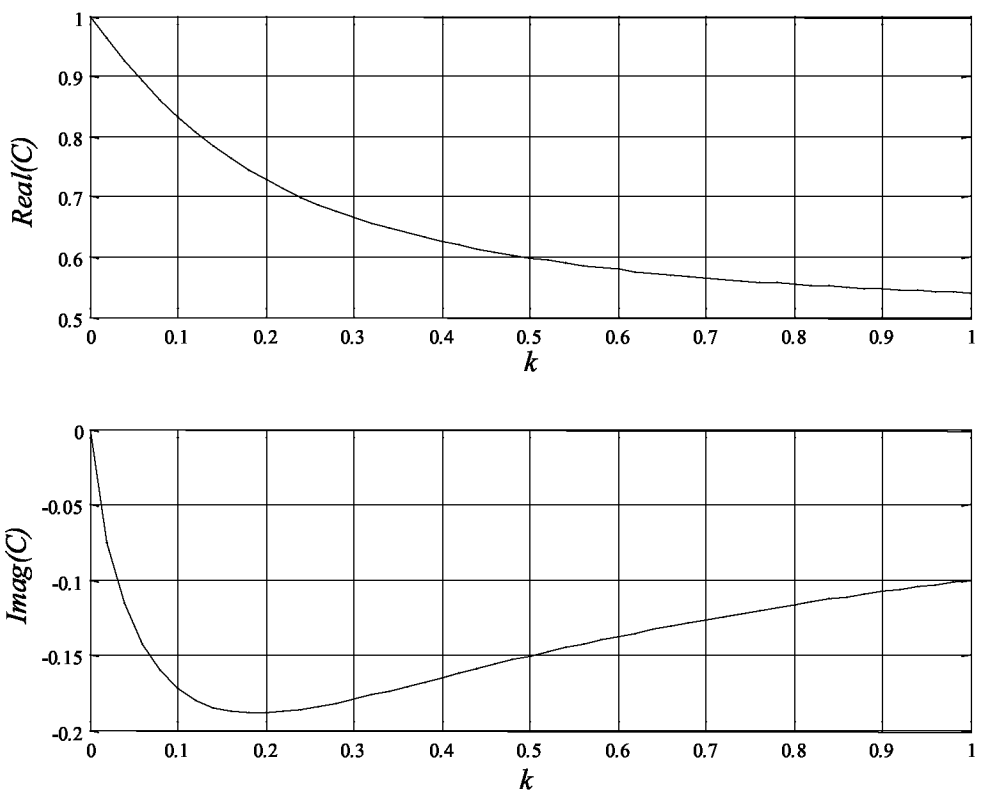

Figure 11-15. Real and imaginary parts of the Theodorsen function $C(k)$ where k is the reduced frequency.

In order to incorporate Equations (11-56) in a finite element procedure for subsequent *complex eigenvalue analysis*, they must be recast in a pseudo time domain form for developing contributions to the finite element mass, stiffness and damping matrices. This can be accomplished by leaving the Theodorsen function as is, but using the explicit ω's in the equations to construct time derivatives, producing the following equations:

$$L = 2\pi\rho U^2 b\left\{\frac{C(k)}{U}\dot{h} + C(k)\alpha + [1 + C(k)(1-2a)]\frac{b}{2U}\dot{\alpha} + \frac{b}{2U^2}\ddot{h} - \frac{b^2 a}{2U^2}\ddot{\alpha}\right\} \quad \text{(11-58a)}$$

$$M = 2\pi\rho U^2 b\left\{\begin{array}{l} d_1\left[\frac{C(k)}{U}\dot{h} + C(k)\alpha + [1 + C(k)(1-2a)]\frac{b}{2U}\dot{\alpha}\right] + d_2\frac{b}{2U}\dot{\alpha} \\ + \frac{ab^2}{2U^2}\ddot{h} - \left(\frac{1}{8} + a^2\right)\frac{b^3}{2U^2}\ddot{\alpha} \end{array}\right\} \quad \text{(11-58b)}$$

Now, using Equations (11-58) with the principle of virtual work, contributions to the finite element stiffness, mass and damping matrices can be developed that include the complex-valued Theodorsen function.

However, before that is done, it is noted that the HAWT blade does not conform to the configuration of an infinitely long uniform wing to which the above equations apply. Rather, such quantities as the semi-chord, b, and the resultant velocity, U, vary significantly along the span of the blade. Moreover, the lift curve slope, which in the above equations is assigned the theoretical value of 2π corresponding to a flat plate, varies with blade span. These variations can be approximated by assembling a conglomerate of uniform blades, wherein the above equations are assumed to be applicable incrementally. Specifically, the quantities mentioned above are represented by a linear variation over the length of the element and included within the integral over the element length associated with the principle of virtual work.

Significant detail can be incorporated in this analysis by refining some of the variable quantities mentioned above. For example, inboard stall for a twisted blade turning in still air might be accommodated by reducing the lift curve slope in that region of the blade. More complicated inflow variations can also be accommodated if they are known *a priori*. However, in comparison with other approximations that have been made in this analysis, these types of refinements are deemed excessive. The simple aeroelastic stability analysis presented here is meant to serve primarily as a common sense check for use during the blade design process.

In matrix notation, the finite element equation to be used for investigating the aeroelastic stability of the wind turbine blade is as follows:

$$\begin{aligned}&[M + M_a(\Omega)]\{\ddot{u}\} + [C_C(\Omega) + C_a(\omega,\Omega)]\{\dot{u}\} \\ &+[K(u_0,\Omega) + K_{tc} + K_{cs}(\Omega) + K_a(\omega,\Omega)]\{u\} = 0\end{aligned} \quad \text{(11-59)}$$

where M is the conventional mass matrix and $K(u_0, \Omega)$ is the stiffness matrix, centrifugally stiffened commensurate with displacements, u_0, resulting from centrifugal loads corresponding to the rotor rotational speed, Ω. The displacement, u, and its time derivatives represent motion about this centrifugally loaded state. The α and h degrees of freedom of Equations (11-58) are included in u.

The blade is modeled with NASTRAN tapered beam (CBEAM) elements (developed by the MSC Software Corp.) that have six degrees of freedom at either end. These elements also have provisions for shear deformation and warping of the cross section, although these features were not used in this analysis. Additional terms are added to the various matrices to provide for rotating coordinate system effects. These are the Coriolis and centrifugal softening terms, $C_C(\Omega)$ and $K_{cs}(\Omega)$, respectively, that will be discussed in detail later. The aeroelastic matrices, $M_a(\Omega)$, $C_a(\omega,\Omega)$ and $K_a(\omega,\Omega)$, all depend on Ω, since the free-stream velocity at any blade radius is governed by it (it is assumed that the rotor is turning in still air). Linear shape functions are used in the development of these aeroelastic matrices.

As a demonstration of the method used to generate the aeroelastic matrices, a single beam element's contribution to K_a is presented in Equation (11-60). The element has a length, l, and is bounded by nodes 1 and 2. The stiffness contribution is due to the α terms of Equations (11-58) and can be developed with the principle of virtual work using only α virtual displacements. Thus, for α varying linearly along the element (i.e. $\alpha(x) = \alpha_1(1-x/l) + \alpha_2 x/l$) the contribution of this single element is as follows:

$$\begin{Bmatrix} L_1 \\ L_2 \\ M_1 \\ M_2 \end{Bmatrix} = \rho \int_0^l a_0(x)U^2(x)b(x)C(k(x)) \begin{bmatrix} \left(1-\frac{x}{l}\right)^2 & \frac{x}{l}\left(1-\frac{x}{l}\right) \\ \frac{x}{l}\left(1-\frac{x}{l}\right) & \left(\frac{x}{l}\right)^2 \\ d_1(x)\left(1-\frac{x}{l}\right)^2 & d_1(x)\frac{x}{l}\left(1-\frac{x}{l}\right) \\ d_1(x)\frac{x}{l}\left(1-\frac{x}{l}\right) & d_1(x)\left(\frac{x}{l}\right)^2 \end{bmatrix} dx \begin{Bmatrix} \alpha_1 \\ \alpha_2 \end{Bmatrix} \tag{11-60}$$

Here the quantity 2π of Equations (11-58), which represents the lift curve slope for a flat plate, is replaced by $a_0(x)$ representing the lift curve slope of an airfoil. This slope varies along the length of the element as does the free stream velocity, U, the semichord, b, the Theodorsen function C, and the distance from the elastic axis to the quarter-chord, d_1. The integral is evaluated numerically. Elemental contributions to M_a and C_a are developed in an entirely similar manner.

Commensurate with the use of the NASTRAN CBEAM element above, the NASTRAN commercial finite element software is used for this aeroelastic stability investigation. The contributions to the stiffness, mass, and damping matrices discussed above are supplied by means of a NASTRAN input option. NASTRAN can accommodate non-symmetric, complex-valued matrices as are required in this effort, and it provides a number of complex eigenvalue solvers for the stability analysis.

In addition to Ω, the aeroelastic matrices, $C_a(\omega,\Omega)$ and $K_a(\omega,\Omega)$, also depend on ω, the natural frequency of the mode shape of interest, which occurs in the argument of the Theodorsen function. Since this frequency is unknown at the onset of the computations an iterative process is required for obtaining accurate results. The iterative procedure developed for the aeroelastic stability analysis of the rotor blade is composed of the following steps:

1. Select a value for Ω .
2. In a quasi-static NASTRAN run, create $K(u_0,\Omega)$ for subsequent eigenvalue analysis.

3. Provide an initial guess for ω or update it from the prior calculation.
4. Using a NASTRAN complex eigenvalue solution procedure, compute modes, frequencies and damping coefficients.
5. Select a mode with a small or negative damping coefficient and return to step 3 with corresponding frequency update.
6. When the prior updated frequency is sufficiently close to the subsequently computed one, either suspend computations or modify Ω and return to step 1.

The end goal in this process is to identify the eigenmode that exhibits a negative damping coefficient for the lowest rotor rotational speed. This speed is designated as the *classical flutter speed* for the blade. A comprehensive approach would be to sequentially investigate the stability of each mode by choosing its frequency as the initial guess for ω, and tracking that frequency over a range of increasing Ω. The flutter speed would then correspond to the lowest value of Ω where the damping becomes negative over the set of modes investigated. In practice, however, the first torsional blade mode produces the lowest values of Ω, coupling with other blade modes (primarily flapwise modes) as the rotational speed increases. Of course it is always prudent to check other modes that appear suspicious during the course of the analysis.

Sample Flutter Calculation

After developing some confidence in the above computational procedure by comparing its results to those of Theodorsen, it was applied to the large relatively soft wind turbine blade shown in the wire-frame illustration of Figure 11-16. This blade, termed the baseline blade, was designed as part of the WindPACT Rotor Design Study [Malcolm and Hansen 2002]. Some characteristics of this blade and the associated rotor are listed in Table 11-5. Q6

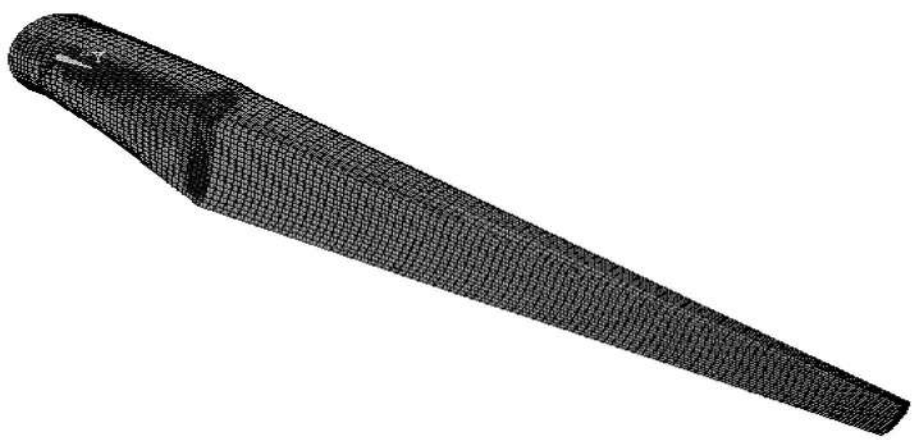

Figure 11-16. Wire-frame illustration of the 1.5 Mw baseline WindPACT blade. [Malcom and Hansen 2002]

Table 11-5.
Characteristics of the Baseline 1.5 MW WindPACT Blade and Rotor

Characteristic	Units	Value
Rated power	MW	1.5
Rotor diameter	m	70
Max rotor speed	rpm	20.5 (0.342 Hz)
Max tip speed	m/s	75
Blade coning	deg	0
Max blade chord	m	8% of radius
Radius to blade root	m	5% of radius
Rotor solidity		0.05
Blade mass	kg	4,230
Hub mass	kg	15,104
Total rotor mass	kg	32,016
1st flapwise frequency	Hz	1.233 (1.199)
1st edgewise frequency	Hz	1.861 (1.714)
2nd flapwise frequency	Hz	3.650 (3.596)
1st torsional frequency	Hz	9.289 (9.846)

Although not readily apparent from Figure 11-16, the blade has a modest amount of twist, from 11.1 deg. at the root to 0.0 deg. at the tip. The modal frequencies in parentheses in this table were computed with the software developed herein with Ω set to zero and the Theodorsen function, $C(k)$, set to 1.0. They differ from the companion frequencies taken from the WindPACT study, which were computed using the ADAMS software (developed by the MSC Software Corp.). The two models are inherently different, yet the frequency differences are small. Only minimal effort was made to minimize these differences.

In Figure 11-17 a planform view of the blade is presented showing the positions of the elastic axis and the axis representing the locus of the cross-sectional center of gravity. As the elastic axis is forward of the mid-chord, the quantity a in Equations (11-59) is negative, varying along the span from – 0.354 to – 0.284. Since in this implementation a constant value of a is required, a mid value of – 0.32 was selected.

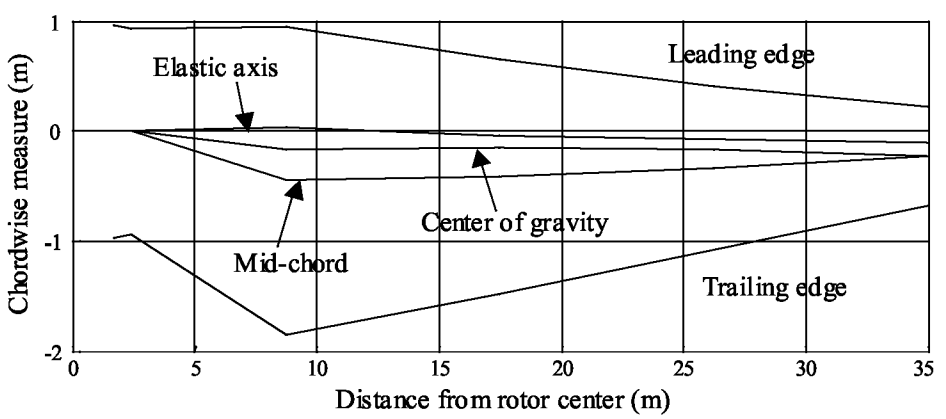

Figure 11-17. Diagram of the planform of the baseline 1.5 MW WindPACT blade showing the locations of the elastic axis and the cross-sectional centers of gravity.

Flutter Analysis Results

Aeroelastic stability predictions with the rotor turning in still air were made for this baseline model. Results indicate that the onset of flutter occurs at a rotational speed of 43.4 rpm (0.723 Hz) which is 2.14 times the maximum design operating speed of the rotor. As shown in Figure 11-18, the mode shape associated with the onset of flutter contains significant amounts of edgewise (motion in the direction of the chord), flapping, and pitching motion. Its frequency of oscillation is 6.234 Hz, which is significantly lower than the 1st torsional frequency of 9.289 Hz.

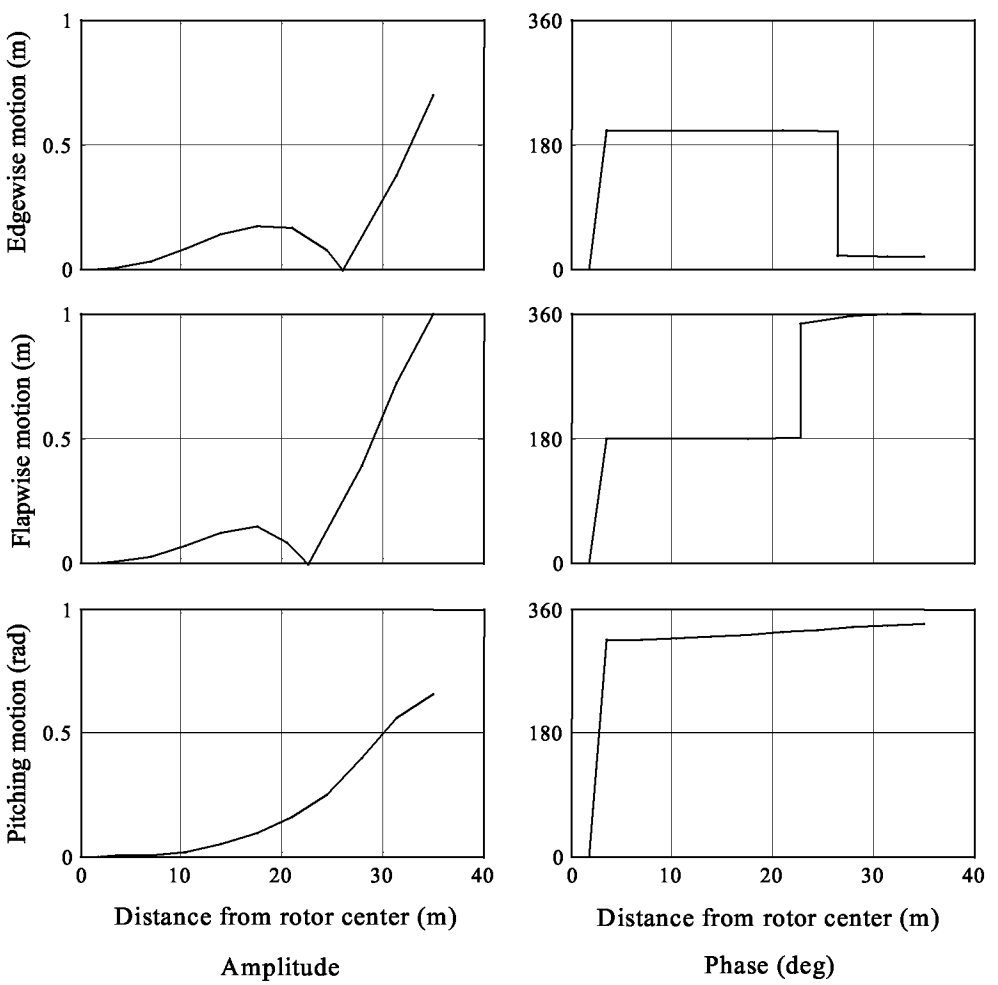

Figure 11-18. Mode shape at the onset of flutter for the 1.5 MW baseline WindPACT uncoupled blade.

In classical flutter, motion in the edgewise direction is generally minimal, and the large amount predicted here is thought to be due to the fact that the blade is twisted, and that the frequency of the second edgewise mode (6.153 Hz) is close to the flutter frequency of 6.234 Hz. The amount of twist in the blade appears to have an important influence on the flutter mode shape. In fact, when flutter predictions are made for an entirely similar blade that is not twisted, edgewise motion in the associated flutter mode is minimal.

According to this analysis, the 2nd flapwise mode combines with the 1st torsional mode to form the flutter mode. This combination of modes was also observed by Hansen [2004] in predicting classical flutter in HAWTs with a software capability he has developed. In contrast, for fixed wing aircraft, it is the 1st flapwise mode that combines with the 1st torsional mode.

Experimental Verification

Unfortunately, no experimental data exist to corroborate these results. However, the flutter analysis technique described herein has been verified by comparison to the observed flutter in a VAWT [Lobitz and Ashwill 1985]. The experimental flutter frequency was measured at 745 rpm [Popelka 1982], reasonably close to the predicted frequency of 680 rpm. The inclusion of a small amount of structural damping in the model greatly improved the agreement. The flutter mode shape was also well predicted using this technique.

References

Adler, F. M., *et al.*, 1980, *Development of an 8 kW Wind Turbine Generator for Residential Type Applications, Phase I - Design and Analysis*, Technical report RFP-3007-2, Vol. II, Bethpage, New York: Grumman Energy Systems, Inc.

Boeing, 1982, *Mod-2 Wind Turbine System Development Final Report, Vol. II: Detailed Report*, NASA CR-168007, DOE/NASA 0002-82/2, Cleveland, Ohio: NASA Lewis Research Center, p. 3-9 to 3-10.

Carne, T. G., D. W. Lobitz, A. R. Nord, and R. A. Watson, 1982, *Finite Element Analysis and Modal Testing of a Rotating Wind Turbine*, Report No. SAND82-0345, Albuquerque, New Mexico: Sandia National Laboratories.

Carne, T. G., J. P. Lauffer, and A. J. Gomez, 1988, *Modal Testing of the Eolé*, SAND87-1506, Albuquerque, New Mexico: Sandia National Laboratories.

Carne, T. G., J. P. Lauffer, A. J. Gomez, and T. D. Ashwill, 1989, "Model Validation Testing of the Sandia 34-meter Test Bed Turbine using Substructure Modal Testing," *Proceedings, ASME Energy Sources Technology Conference and Exhibition and 7th Intersociety Cryogenic Symposium*, New York: American Society of Mechanical Engineers.

Carne, T. G., and G. H. James, 2008, "The Inception of OMA in the Development of Modal Testing Technology for Wind Turbines," Keynote Address at 2007 International Operational Modal Analysis Conference, to be published in *Mechanical Systems and Signal Processing*.

Dohrmann, C. R. and P. S. Veers, 1989, "Time Domain Response Calculations for Vertical Axis Wind Turbines", *Proceedings of the 8th ASME Wind Energy Symposium*, Houston, TX.

Dowell, E. E. (Editor), 1995, *A Modern Course in Aeroelasticity*, Kluwer Academic Publishers: Dordrecht, pp. 217-227.

Dym, C. L., and I. H. Shames, 1973, *Solid Mechanics: A Variational Approach*: McGraw Hill: pp. 164-176.

Franklin, J. N., 1968, *Matrix Theory*, Englewood Cliffs, New Jersey: Prentice-Hall Inc., p. 99.

Fung, Y. C., 1969, *An Introduction to the Theory of Aeroelasticity*, Dover Publications Inc., New York, pp. 210-216.

Hansen, M. H., 2004, "Stability Analysis of Three-Bladed Turbines Using an Eigenvalue Approach," *Proceedings of the 2004 ASME/AIAA Wind Energy Symposium*, Reno, pp. 192-202.

James, G. H., T. G. Carne, and J. P Lauffer, 1993, "The Natural Excitation Technique (NExT) for Modal Parameter Extraction from Operating Wind Turbines," SAND92-1666, Albuquerque, New Mexico: Sandia National Laboratories.

James, G. H., 1994, "Extraction of Modal Parameters from an Operating HAWT using the Natural Excitation Technique (NExT)," *Proceedings, 13th ASME Wind Energy Symposium*, New York: American Society of Mechanical Engineers.

James, G. H., T. G. Carne, and J. P. Lauffer, 1995, "The Natural Excitation Technique (NExT) for Modal Parameter Extraction from Operating Structures," SEM *International Journal of Analytical and Experimental Modal Analysis*, Vol. 10, No. 4.

James, G. H., T. G. Carne, and P. S. Veers, 1996, "Damping Measurements Using Operational Data," *ASME Journal of Solar Energy Engineering*, Vol. 18, No. 3, New York: American Society of Mechanical Engineers.

Klahs, J. W., Jr., and J. H. Ginsburg, 1979, "Resonant Excitation of a Spinning, Nutating Plate," *Journal of Applied Mechanics*, Vol. 46: pp. 132-138.

Klosterman, A. L., and R. Zimmerman, 1975, *Modal Survey activity Via Frequency Response Functions*, SAE Paper No. 751068: Society of Automotive Engineers.

Lauffer, J. P., 1986, "The Statistical Variation of Modal Parameters within Production Units," *Proceedings, 4th International Modal Analysis Conference*, Los Angeles, California.

Leishman, J. G., 2002, "Challenges in Modeling the Unsteady Aerodynamics of Wind Turbines," *Wind Energy*, 5, pp. 85-132.

Lindenburg, C., and H. Snel, "PHATAS-II: Program for Horizontal Axis Wind Turbine Analysis and Simulation, Version II," *Proceedings, Twelfth ASME Wind Energy Symposium*, SED-Vol. 14, New York, NY: American Society of Mechanical Engineers, pp. 133-138.

Lobitz, D. W., and T. D. Ashwill, 1985, "Aeroelastic Effects in the Structural Dynamic Analysis of Vertical Axis Wind Turbines," *Proceedings, Windpower '85*, San Francisco, CA, pp. 82-88.

Lobitz, D. W., 2004, "Aeroelastic Stability Predictions for a MW-Sized Blade," *Wind Energy*, Vol. 7, pp. 211-224.

Malcolm, D. J., and A. D. Wright, 1994, "The Use of ADAMS to Model the AWT-26 Prototype," *Proceedings, Wind Energy - 1994 Symposium*, SED-Vol. 15, W. Musial *et al.*, eds., New York: American Society of Mechanical Engineers, pp. 125-131.

Malcolm, D. J. and G. H. James, 1995, "Stability of a 26m Teetered, Free-Yaw Wind Turbine," *Proceedings, 10th ASCE Engineering Mechanics Conference*: American Society of Civil Engineers.

Malcolm, D. J., and A. C. Hansen, 2002, "WindPACT Rotor Turbine Design Study," NREL/SR-500-32495, Golden, Colorado: National Renewable Energy Laboratory.

Ottens, H. H., and R. J. Zwaan, 1978a, *Description of a Method to Calculate the Aeroelastic Stability of a Vertical Axis Wind Turbine*, NLR TR 78072 L, The Netherlands: National Aerospace Laboratory.

Ottens, H. H., and R. J. Zwaan, 1978b, "Investigation of the Aeroelastic Stability of a Vertical Axis Wind Turbine," *Proceedings, Second International Symposium on Wind Energy Systems*, Paper C3, The Netherlands.

Patel, J. S., and S. M. Seltzer, 1971, *Complex Eigenvalue solution to a Spinning Skylab Problem*, Vol. II, NASA TMX-2378, Houston, Texas: NASA Johnson Space Flight Center.

Popelka, D., 1982, *Aeroelastic Stability of a Darrieus Wind Turbine*, SAND82-0672, Albuquerque, New Mexico: Sandia National Laboratories.

Rumsey, M., J. Hurtado, B. Hansche, T. Simmermacher, T. Carne, and E. Gross, 1997, "In-Field Use of Laser Doppler Vibrometer on a Wind Turbine Blade," *Sound and Vibration*, Vol. 32, No. 2, p 14-19.

Sweeney, T. E., and W. B. Nixon, 1978, *Two-Dimensional Lift and Drag Characteristics of Grumman Windmill Blade Section*, (unpublished), Princeton, New Jersey: Princeton University.

Spera, D. A., 1975, *Structural Analysis of Wind Turbine Rotors for NSF-NASA Mod-0 Wind Power System*, NASA TM X-3198, Cleveland, Ohio: NASA Lewis Research Center.

Spera, D. A., 1977, "Comparison of Computer Codes for Calculating Dynamic Loads in Wind Turbines," NASA TM-73773, Cleveland, Ohio: NASA Lewis Research Center.

Sullivan, T. L., 1981, "A Review of Resonance Response in Large, Horizontal-Axis Wind Turbines," *Proceedings, Wind Turbine Dynamics Workshop*, R. W. Thresher, ed., NASA Conference Publication 2185, DOE Publication CONF-810226, Cleveland, OH: NASA Lewis Research Center, pp. 237-244.

Theodorsen, T., 1935, "General Theory of Aerodynamic Instability and the Mechanism of Flutter," NACA Report 496, Washington, DC: National Advisory Committee for Aeronautics.

Thresher, R. W., A. D. Wright, and E. L. Hershberg, 1986, "A Computer Analysis of Wind Turbine Blade Dynamic Loads," *Journal of Solar Energy Engineering*, Vol. 108: pp. 17-25.

Vollan, A. J., and R. J. Zwaan, 1977, *Contribution of NLR to the First Phase of the National Research Program on Wind Energy, Part II: Elastomechanical and Aeroelastic Stability*, NLR TR 77030 U Part II, The Netherlands: National Aerospace Laboratory.

Warmbrodt, W., and P. Friedmann, 1980, "Coupled Rotor/Tower Aeroelastic Analysis of Large Horizontal Axis Wind Turbines," *AIAA Journal*, Vol. 18, No. 9: pp. 1118-1124.

Wright, A. D., M. L. Buhl, and R. W. Thresher, 1988, *FLAP Code Development and Validation*, SERI/TR-217-3125, Golden, Colorado: National Renewable Energy Laboratory.

Author Query Form

(Queries are to be answered by the Author)

ASM Wind Turbine – Chapter 11

The following queries have arisen during the typesetting of your manuscript. Please answer these queries.

Query Marker	Query	Reply
Q1	There is no equation 15. Please check if this should be equation 15 instead.	
Q2	There is no equation 22. Please check if the equations from hereon should be renumbered.	
Q3	There is already equation 33a-c. Please check.	
Q4	This figure is of poor quality. Please check.	
Q5	Equations and their citations were renumbered from here. Please check if correct.	
Q6	This was changed to Table 5. OK?	

Thank you very much.